Chemical Geology 660 (2024) 122151

Contents lists available at ScienceDirect

Chemical Geology

journal homepage: www.elsevier.com/locate/chemgeo

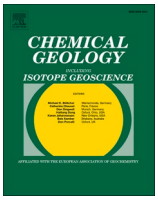

Rare-earth element (REE) remobilization and fractionation in bauxite zones from sedimentary kaolin deposits, western Georgia (USA), Upper Coastal Plain

Anthony Boxleiter [a,*], Yinghao Wen [b], Yuanzhi Tang [b], W. Crawford Elliott [a]

[a] Department of Geosciences, Georgia State University, 38 Peachtree Center Ave., Atlanta, GA 30303, USA
[b] School of Earth and Atmospheric Sciences, Georgia Institute of Technology, 311 Ferst Dr., Atlanta, GA 30332, USA

ARTICLE INFO

Keywords:
Gibbsite
Kaolin
Bauxite
Georgia
Rare-earth elements

ABSTRACT

Rare-earth elements (REE) are critical minerals that are indispensable for high-tech products and technologies. Significant efforts have been focused on the exploration and identification of new and domestic reserves of REE. This study reports geochemical and mineralogical occurrences of accumulated REE with significant fractions of ion-adsorption clays (IAC) within bauxite-kaolin ore, hosted within sedimentary strata. This deposit type can be found throughout portions of Georgia and eastern Alabama (USA) in the Southeast Upper Coastal Plain. These deposits were developed by high degrees of chemical weathering of older, kaolinite-rich sedimentary strata. Several major changes in whole rock mineralogy and geochemistry occurred, leading to the development of zones of REE depletion, fractionation, and accumulation. Depletions of REE in the bauxite zone were significant, with whole rock contents of ~50% ΣREE relative to average upper continental crust (UCC). Fractionated REE were observed by low La/Yb_N values ($La/Yb_N = 0.2$) due to depletion in LREE (<40% UCC) with concomitant HREE retention (~1.1–1.3 times UCC). Strongly positive Ce/Ce* anomalies (Ce/Ce* = 1.3), very low ion-exchangeable Ce contents (Ce/LREE = 0.1), and low solubility of Ce (0.9–1.2%) under reducing conditions compared to all other LREE (4.5–9.9%) were further observed. These characteristics were strong indications of REE fractionation that occurred during formation of the bauxite zone. Underlying the bauxite zone, accumulations of the remobilized REE were substantial. At the base of the lower kaolin zone, elevated ion-exchangeable REE contents were notable (11–33% for total REE), and more specifically 11–12% for LREE, ~28% for ΣTb-Lu, and ~ 33% for Y. The elevated ion-exchangeable contents coincided with whole rock contents that were ~ 250% ΣREE relative to UCC. These REE accumulations occurred within organic-rich strata at the base of the section. This setting represents a significant difference relative to the REE accumulations in profiles for the granite-regolith deposit type. These findings highlighted the movement of dissolved REE, accumulation as sorbed species, as well as the potential role that organic ligands play during REE precipitation and sorption processes. These results permit consideration for further research into REE occurrences in clay deposits of sedimentary origin, which have been underexplored compared to granite-regolith REE deposits.

1. Introduction

The rare-earth elements (REE) include Sc, Y, and the lanthanide series (IUPAC: Connelly et al., 2005). The growing high demand of REE in the high-tech and clean energy industries continues to bring attention to global supply constraints (Long et al., 2010). The United States Geological Survey (USGS) considers REE as critical mineral resources, with the lanthanide series of light REE (LREE) and heavy REE (HREE) grouped as La—Gd and Tb—Lu, respectively (Van Gosen et al., 2019; Fortier et al., 2018). Y and Sc are considered HREE (Teitler et al., 2019; Bern et al., 2016; Bunzli, 2013; Chakhmouradian and Wall, 2012; Tepe and Bau, 2016; Mioduski, 1993).

The REE are commonly grouped together due to their similarity in properties and co-occurrences in mineral resource deposits and other geochemical systems. The LREE are typically higher in concentration compared to HREE within the average composition of the Earth's upper continental crust (UCC; Rudnick and Gao, 2003). Chemical weathering of rocks and sediments at the Earth's upper crust causes the release of

* Corresponding author.
E-mail address: aboxleiter1@student.gsu.edu (A. Boxleiter).

https://doi.org/10.1016/j.chemgeo.2024.122151
Received 24 February 2024; Received in revised form 9 April 2024; Accepted 8 May 2024
Available online 9 May 2024

REE into weathering solutions and natural waters (Li et al., 2020; Xu et al., 2017; Sanematsu et al., 2015; Feng et al., 2011; Aubert et al., 2001; Taunton et al., 2000; Middelburg et al., 1988). Dissolved REE can adsorb onto mineral surfaces or precipitate as secondary REE minerals, which may selectively enrich individual REE, LREE, and/or HREE, and subsequently induce REE fractionation relative to their parent sources. These fractionation patterns outline the geological and biogeochemical mechanisms leading to the enrichment or depletion of the REE relative to UCC values.

Ion-adsorption clay (IAC) deposits are those hosting REE enrichments predominantly associated with clay-rich rocks. IAC deposits represent >50% of the global supply of HREE mined (Van Gosen et al., 2019; Li et al., 2017; Yang et al., 2013; Chi and Jun, 2011; Wu et al., 1996; Wu et al., 1990). REE are commonly extracted from IAC deposits through "solution" mining such as batch, heap, or in-situ leaching methods (Brahim et al., 2022; Borst et al., 2020; Long et al., 2020; He et al., 2016; Xiao et al., 2015; Moldoveanu and Papangelakis, 2012, 2013, 2016). Early generations of industrial-scale resource extraction operations used concentrated NaCl leaching solutions before $(NH_4)_2SO_4$ solutions became more common due to higher desorption efficiency. The REE are ion-exchangeable in IAC deposits, and their extractability is driven by the differences in hydration enthalpy between the REE and the exchanging ion (e.g. Na^+, NH_4^+). Lab-scale ion-exchange experiments are commonly used to study these REE. The quantity and type of ion-exchangeable REE can therefore be determined from different IAC sources or geologic deposit types.

Weathered granites (granite-regolith) are known to host IAC deposits (Li and Zhou, 2020, Li et al., 2017, 2019, Li et al., 2020, Li and Zhou, 2020; Xu et al., 2017; Sanematsu and Watanabe, 2016; Chi and Jun, 2011; Bao and Zhao, 2008; Wu et al., 1990; Ren, 1985). The granite-regolith deposit type is typified by thick weathering profiles over granitic bedrock. Studies have shown that ion-exchangeable REE accounts for approximately 80% of the total REE in the regolith-hosted, weathered crust deposit type (He et al., 2016; Ruan et al., 2005). These deposits, their clay mineral assemblage, and ion-exchangeable REE contents are the product of the weathered regolith and dissolved REE. Clay minerals, such as kaolinite, are formed during the weathering of granitic rock containing primary minerals such as feldspars. The source of the dissolved REE may be from weathered REE-minerals in these rocks, which subsequently form hydrated complexes that are capable of adsorbing onto clay mineral surfaces (Text S1). Accumulations of these REE with clays contributes to the overall ion-exchangeable contents of these deposits.

Compared to granite-regolith type REE deposits, bauxite-kaolin (sedimentary-hosted) type deposits have been underexplored for their connection to REE. The genesis of these -bauxite-kaolin ores hosted within sedimentary strata, and their REE accumulations, are open questions. This present study examined the mineralogy, geochemistry, and REE contents from a bauxite-kaolin deposit, western Georgia (USA), Upper Coastal Plain. The deposit was characterized by zones of REE depletion, fractionation, and accumulation. Several noteworthy differences and similarities in REE contents were observed between this deposit and the granite-regolith deposit type, providing insight into future exploration for REE resources.

2. Materials and methods

2.1. Geologic Background

In the Andersonville district, western Georgia, bauxite occurs as thin (1–5 m) and flat-tabular bodies within larger lenses (10 m or more) of sedimentary kaolin of the Paleocene-Eocene Nanafalia Formation (Wilcox Group; Cofer and Manker, 1983; Burst, 1974; Zapp, 1965). Typically, these bauxite-kaolin ore bodies are hosted within the sand-dominated sequences of the Nanafalia Formation, and in turn are overlain by the Tuschoma Formation (Fig. 1). Lignitic (organic-rich), clayey materials are common at the lithologic transitions of the bauxite-kaolin ore bodies with the underlying sandy portions of the Nanafalia Formation (Lukas et al., 1983; Zapp, 1965). Unconformably underlying the Nanafalia Formation is the limestone of the Paleocene Clayton Formation (Cofer and Manker, 1983; Warren and Clark, 1965).

Similar occurrences of these bauxite-kaolin deposits are also present in eastern Alabama (Eufaula district) and central Georgia. The deposits in the Eufaula district are similarly associated with the Nanafalia Formation. However, the deposits in the Eufaula district are smaller, laterally discontinuous and scattered. Due to extensive erosion and karst topography of the underlying Clayton limestone, slumping of the overlying strata was accompanied by distortion, truncation, and faulting of

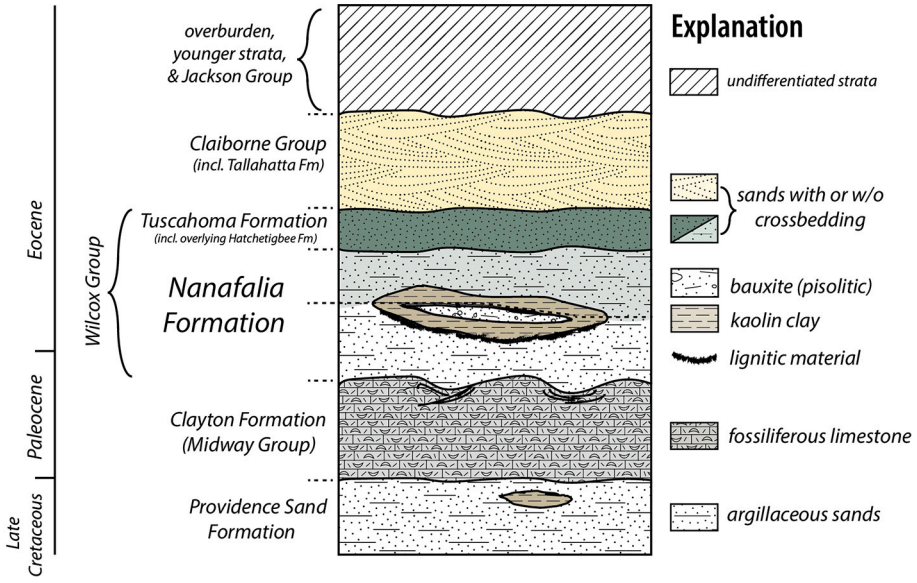

Fig. 1. Generalized schematic of the deposit model for the Nanafalia Formation bauxite-kaolins and adjacent strata (*after* Cofer and Manker, 1983; Austin, 1972; Zapp, 1965). The Providence Sand Formation is the oldest formation exposed in the Andersonville district. Unconformities are traced by dashed lines. The Federal Geographic Data Committee (FGDC) standard for digital cartography and symbolization was referenced for USGS-compliant lithologic patterns. Formation thicknesses are not to scale.

the bauxite-kaolin ore bodies (Burst, 1974; Warren and Clark, 1965). On the other hand, bauxite-kaolin deposits in the central Georgia region, southern Wilkinson County, are hosted by age-equivalent strata of the Oconee Group (Nystrom et al., 1991; Huddlestun, 1982). Across the UCP, the bauxite beds are always hosted within the larger lenses of kaolin. These bauxites are thought to have been formed during the same period across the region (Austin, 1972; Smith, 1929).

The Piedmont crystalline rocks, including granites and gneisses rich in feldspars and micas, were the primary source of eroded siliciclastics building out the Coastal Plain along the Fall Line trend during the late Mesozoic to Cenozoic Eras (Fig. 2; Murray, 2007; Pavich, 1989; Owens and Gohn, 1985; Hack, 1982; Hinckley, 1965). Sedimentary kaolin beds were formed within the UCP, proximal to the Fall Line. These deposits were formed through deposition of kaolinitic sediments and subsequent in-situ weathering. In some places, these kaolin beds were subjected to subaerial erosion and weathering that resulted in the formation of the bauxite (Cofer and Manker, 1983; Austin, 1972; Lang et al., 1965; Stull and Bole, 1926). In the central Georgia region, these bauxites formed in association with the upper strata of the late Cretaceous Buffalo Creek Member kaolins (Austin, 1972; Lang et al., 1965; Stull and Bole, 1926). The Buffalo Creek Member (Gaillard Formation, Oconee Group) contained pisolites, diagnostic concretionary features of bauxite formation (Huddlestun and Hetrick, 1991; Austin, 1972). These bauxites were later overlain by younger kaolinitic sediments during the Eocene, with minor amounts of reworked and/or resilicated bauxitic material (Cofer and Manker, 1983; Austin, 1972; Smith, 1929).

2.2. Materials

This study examined geologic drill core samples of bauxite-kaolin ore from the Andersonville district located in western Georgia. Samples were recovered from a 5 cm diameter core from a section of a bauxite-kaolin deposit. The section of bauxite-kaolin was intersected across a depth of approximately 12 to 21 m from the surface. The middle portion of the section showed diagnostic characteristics of bauxite rock, including a friable texture and the presence of pisolites. Previous reports on the Andersonville district's deposits of bauxite-kaolin generally defined the bauxite zones with gibbsite mineral contents exceeding kaolinite (Zapp, 1965).

Samples consisted of intervals (0.75 m in length) from the section (9 m thick), comprising a total of 12 samples for study. The sample labels ranged from AND-10-605 to AND-10-617. These samples were crushed, split, and milled to fine-grained mineral powders. Two leaching experiments were conducted to evaluate the modes of REE occurrence. Pristine and reacted samples were analyzed for mineralogy and chemical composition, as detailed below.

2.3. Solid Sample analyses

2.3.1. X-ray diffraction (XRD)

The mineralogical composition of solid samples was analyzed by XRD using a Panalytical Empyrean diffractometer with Cu Kα radiation (1.5406 Å) and Ni filter. The detection limit was ~1 wt% for a given mineral. Data processing and phase identification used the MDI-JADE software (version 8.3) and International Center for Diffraction Data

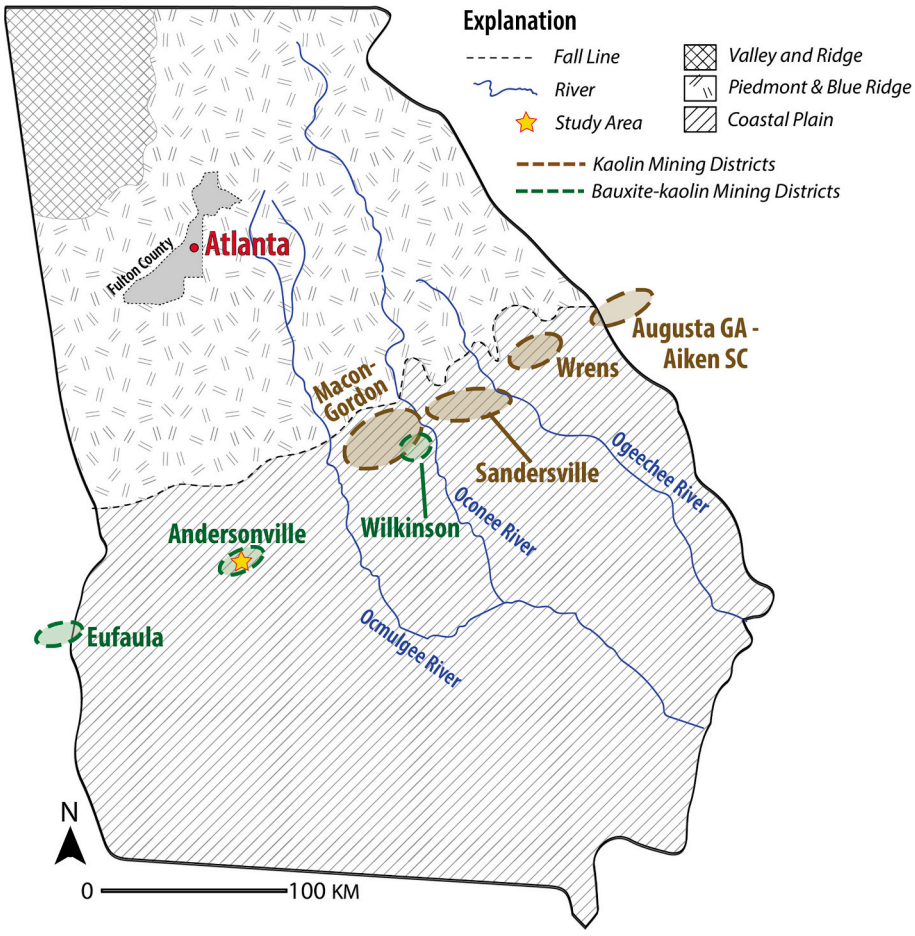

Fig. 2. State map of Georgia showing major geologic provinces and mining districts (*after* Patterson and Murray, 1984), sampling location from the Andersonville district, and the western Georgia UCP region separated from central and eastern regions by the Ocmulgee and Ogeechee Rivers, respectively.

(ICDD) PDF-4+ 2021 reference databases.

2.3.2. Thermogravimetric analysis (TGA)

TGA was performed using a Perkin Elmer TGA8000 instrument at 50 °C/min over 50–1000 °C and the data is presented in Table 1. The total weight loss measured over 50–1000 °C provided the loss-on-ignition (LOI) value for normalizing and reporting chemical analyses. These materials did not contain halloysite, which typically shows thermal decomposition due to dehydration at <120 °C (Minato, 1988). The diagnostic weight losses due to dehydroxylation were recorded for gibbsite over the temperature range ~200–450 °C, and ~450–750 °C for kaolinite (Wilson, 2013; Zhu et al., 2010; Kloprogge et al., 2002). Gibbsite and kaolinite contain hydroxyl groups which account for ~35 wt% and ~14 wt% of the structure, respectively. Thermal decomposition and weight loss as H_2O occur at ~200–450 °C and >450 °C, respectively. The weight losses attributed to gibbsite and kaolinite were used to estimate their contents (Table 2).

2.3.3. X-ray Fluorescence (XRF)

Solid samples were prepared by total digestion via lithium borate fusion for major/minor elemental analysis and pressed pellets for trace element analysis (Text S2) using a Rigaku Primus IVi wavelength-dispersive sequential XRF. Duplicates and measurement of certified reference materials were conducted to monitor reproducibility and verify accuracy (Table S2–4).

2.3.4. Carbon and sulfur analysis

Carbon and sulfur concentrations were measured using a LECO SC832DR carbon and sulfur analyzer. These measurements were conducted at 1450 °C with stable baselines held at 1350 °C prior to each analysis. Samples, standards, and blanks were prepared in ceramic combustion vessels (Leco product no. 528–203). Starting weights of 0.50 g (+/− 0.01) were used for samples and standards. Prepared weights of the samples and standards were mixed with 1.5 g (+/− 0.1) combustion reagent "COM-CAT" (Leco product no. 502–321). Standards measurements were recorded against the measured values of certified reference materials to verify accuracy (Table S3).

2.3.5. Weathering Index

Weathering indexes, such as the Chemical Index of Alteration or CIA (Eq. 1; Nesbitt and Young, 1982), utilize whole rock chemical analyses results for major and minor oxides (molar basis). The inception of the CIA index was based on the analyses of clay-rich sediments (Text S3). High CIA values correspond to high degrees of weathering. Values near 100% represent a residuum considered completely weathered from parent rock minerals (Voicu and Bardoux, 2002).

$$CIA = \frac{(Al_2O_3)}{(Al_2O_3 + CaO + Na_2O + K_2O)} \text{ x } (100) \quad (1)$$

2.3.6. Normalization to Upper Continental Crust (UCC)

The measured REE concentrations were presented as both absolute values and normalized values relative to average UCC (Rudnick and Gao, 2003; Wall, 2021). Such normalization shows gains and losses of elements resulting from weathering (and other processes) acting on crustal bedrock. The process of normalization also smooths the erratic patterns of absolute elemental concentrations due to Oddo-Harkins rule (Migaszewski and Gałuszka, 2015; Chakhmouradian and Wall, 2012).

2.3.7. Ce anomaly calculations

Ce anomalies (Ce/Ce*) were tracked in this study and in similar studies due to the unique redox behavior of Ce in the weathering environment (Xu et al., 2017; Sanematsu et al., 2015; Ma et al., 2011). Anomalies were calculated based on the relative concentrations of Ce with respect to neighboring REE (Eq. 2; Bao and Zhao, 2008, McLennan and Taylor, 2012). Values of Ce/Ce* <1.0 represent negative anomalies, and Ce/Ce* values >1.0 are positive anomalies (Verplanck et al., 2014).

$$\frac{Ce}{Ce^*} = \frac{Ce_N}{\left(La_N^{1/2} * Pr_N^{1/2}\right)} \quad (2)$$

2.4. Chemical Extractions

2.4.1. Extraction methods

Two chemical extraction methods were used to determine different REE inventories in the bauxite-kaolin materials: ion-exchange and sequential extraction. Details of the ion-exchange method are in Text S4 and this method is commonly applied to determine the fraction of ion-exchangeable REE (Long et al., 2020; He et al., 2016; Xiao et al., 2015; Moldoveanu and Papangelakis, 2012, 2013). The sequential extraction method consisting of three stages: Stage 1 for the extraction of REE in acid-soluble phases (e.g. carbonate minerals), Stage 2 for reducible phases (e.g. Fe-oxides), and Stage 3 for oxidizable phases (e.g. sulfide minerals, organics; *after* Tessier et al., 1979; Text S5).

2.4.2. Solution phase analysis

Solutions from the ion-exchange and sequential extraction were analyzed using an Agilent 7500a inductively coupled plasma mass spectrometry (ICP-MS). The plasma was created by ionizing argon gas. The measured analytes included ^{45}Sc, ^{89}Y, ^{139}La, ^{140}Ce, ^{141}Pr, ^{146}Nd, ^{147}Sm, ^{153}Eu, ^{157}Gd, ^{159}Tb, ^{163}Dy, ^{165}Ho, ^{166}Er, ^{169}Tm, ^{172}Yb, ^{175}Lu, and non-REE elements ^{55}Mn and ^{56}Fe. Calibration standard solutions were re-measured after every 30 samples to ensure data accuracy. Method "blank" solutions and replicates were tabulated with results (Table S6, S7).

The % exchangeable REE were determined for each REE on a solid-solid and solid-leachate basis. The % exchangeable REE were calculated based on REE concentrations in the initial whole rock (C_{wr}) and solid phase residue following ion-exchange (C_{spr}; Eq. 3).

$$\%\text{Exchangeable}_{\text{solid-solid}} = \frac{C_{wr} - C_{spr}}{C_{wr}} \times 100 \quad (3)$$

The leaching efficiency (Eq. 4; Wen et al., 2023) was calculated to determine % exchangeable REE on a solid-leachate. This equation was also applied to leachates analyzed from the sequential extraction analyses. C_1 and C_0 are the analyte concentrations for the leachate and whole rock samples, respectively. V_1 (mL) is the volume of the leaching solution and m_0 (grams) is the mass of whole rock sample used per specimen vial. The V_1 value for ion-exchange was 200 mL and the V_1 values sequential extractions were 16, 20, and 13 mL for Stage 1, Stage 2, and Stage 3, respectively. The m_0 for the ion-exchange was 5.0 g and for the sequential extractions each stage used 0.5 g.

Table 1
TGA results and thermogravimetric losses (values in wt%) per sample and temperature ranges.

Sample ID	AND 605	AND 606	AND 607	AND 608	AND 609	AND 610	AND 617	AND 611	AND 612	AND 613	AND 614	AND 615
<200 °C	1.07	<0.10	<0.10	0.53	0.55	0.25	0.11	0.10	0.10	0.33	0.38	1.35
200–450 °C	<0.10	5.80	11.84	11.69	23.04	11.98	12.90	9.12	1.83	<0.10	<0.10	1.49
>450 °C	14.19	11.3	9.11	9.33	5.01	9.17	8.80	10.08	12.56	13.25	13.37	12.69

Table 2
Gibbsite (wt%), kaolinite (wt%), and CIA values (%) of the samples.

	Upper Kaolin Zone			"Bauxite Zone"					Lower Kaolin Zone			
Sample ID	AND 605	AND 606	AND 607	AND 608	AND 609	AND 610	AND 617	AND 611	AND 612	AND 613	AND 614	AND 615
Gibbsite	0	17	34	34	67	35	37	26	5	0	0	1
Kaolinite	97	81	63	64	31	63	60	72	91	97	97	93
CIA	99.18	99.39	99.50	99.64	99.83	99.71	99.64	99.64	99.57	99.62	99.33	99.02

$$\text{Leaching efficiency } (\%) = \frac{C_1 \bullet V_1}{C_0 \bullet m_0} \times 100 \quad (4)$$

2.4.3. Solid phase analysis

Reacted solid residues were analyzed by XRD as described previously. XRF determined elemental composition of the solid phase residues were used to monitor the uptake of the exchanged Mg ions.

3. Results

3.1. Whole rock mineralogy

Kaolinite and gibbsite are the predominant minerals identified on a whole rock basis by XRD (Fig. 3 and S2). Gibbsite was identified using the diagnostic diffraction peaks at 4.8 and 3.1–3.4 Å. Gibbsite content increased from 0% at the top of the bed (upper kaolin zone) to up to 67 wt% in the center of the bed ("bauxite zone"), followed by a gradual decrease to 0% at the bottom of the bed (lower kaolin zone, Table 2). Kaolinite was identified from the diffraction peaks at 7.1, 3.6, and 2.6 Å. Diffraction peaks in the range of 4.1–4.4 Å showed overlap between kaolinite and gibbsite.

Minor amounts of anatase (TiO_2) were identified by XRD (3.5 Å; Fig. 3) across all samples, showing more intense reflections (higher abundance) in samples with elevated gibbsite content. Increasing gibbsite content corresponds with decreasing kaolinite content (Lukas et al., 1983). The peak overlap between anatase (3.5 Å) and kaolinite (3.6 Å) was notably less significant when kaolinite content was lower. Zircon ($ZrSiO_4$), REE-bearing phosphates (e.g. monazite, xenotime), or Fe-oxyhydroxide minerals (e.g. hematite, goethite) were below XRD detection limit (~1 wt%). Trace amounts of alunite (3.0 Å) were identified only in the samples of the upper kaolin zone. Trace amounts of muscovite (~10 Å, Fig. S2) were identified only in the lowermost sample of the lower kaolin zone. XRD results showed no halloysite content or other possible mineral phases present which may have contributed to the TGA analyses and weight losses recorded over the range ~200–450 °C (used to estimate gibbsite mineral content).

3.2. Whole rock composition: Major/minor oxides

The bauxite-kaolins contained SiO_2 (11.60–45.86 wt%) and Al_2O_3

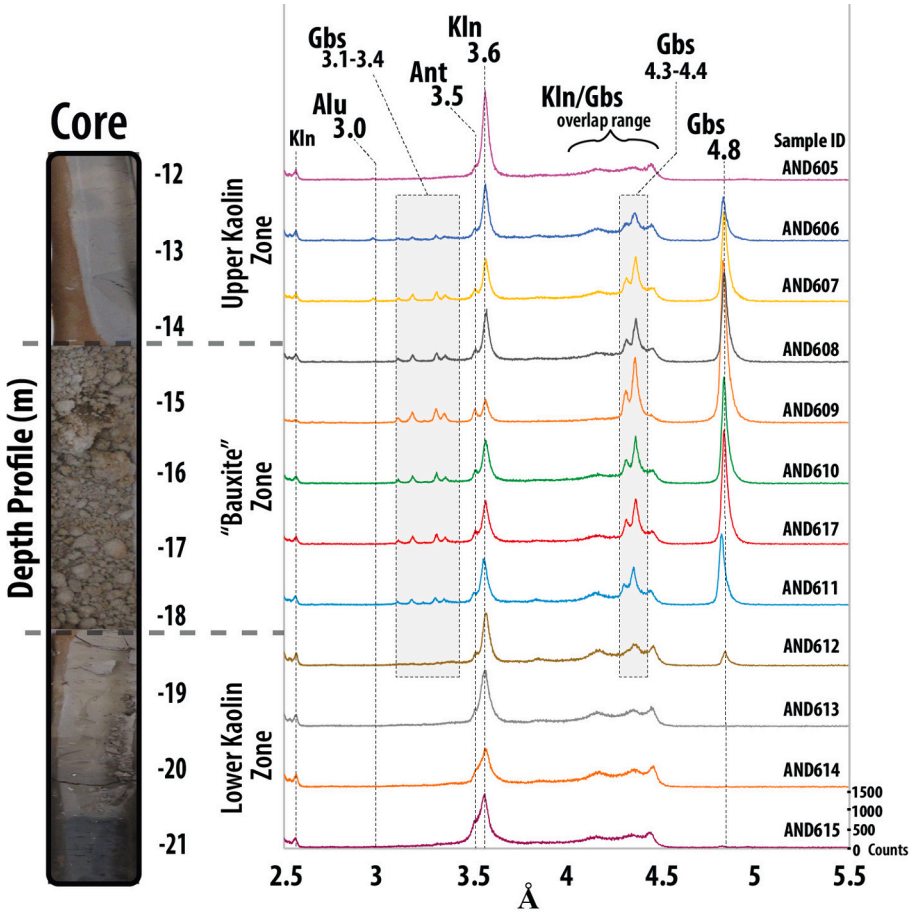

Fig. 3. XRD mineralogical analyses. Kln: kaolinite; Gbs: gibbsite; Ant: anatase; Alu: alunite.

(36.51–55.52 wt%) as the predominant major element oxides (Table 3, Table S2), consistent with the predominant mineral composition of gibbsite and kaolinite per mineralogical analyses (Fig. 3, Table 2). TiO_2 (1.30–2.52 wt%), Fe_2O_3 (0.41–1.08 wt%), and K_2O (0.01–0.19 wt%) were the only major element oxides present in concentrations >0.1 wt%. Overall, TiO_2 and Al_2O_3 concentrations were enriched ~2–5 times relative to Upper Continental Cust (UCC; Table S2) throughout this section.

The enrichments in TiO_2 (1.30–2.52%) and Zr (40–435 ppm) trended positively with gibbsite (0–67 wt%) and CIA values (99.0–99.8%) throughout the section (Table 3, Table 4, Fig. 4). Increasing TiO_2 concentrations throughout the bauxite zone corresponded with anatase mineral contents per XRD analyses and more intense reflections at 3.5 Å (Fig. 3). While Zr concentrations indicated zircon ($ZrSiO_4$), the zircon contents were below XRD detection limit (~1 wt%).

Fe_2O_3 (0.41–1.08 wt%) contents were low throughout the section. Fe-oxyhydroxide minerals were below the XRD detection limit (~1 wt %). Fe_2O_3 contents trended inversely with gibbsite content, CIA values, TiO_2 and Zr (Table 3, Table 4). However, Fe_2O_3 contents showed somewhat positive correlation with Sc contents (Pearson correlation coefficient, Rodgers and Nicewander, 1988; Pearson $r = 0.49$). The highest K_2O (0.19 wt%) and S (~4500 ppm) concentrations corresponded to the presence of trace amounts of alunite ($KAl_3[SO_4]_2[OH]_6$) from upper kaolin zone samples (Fig. 3, Fig. S4). Elevated K_2O (0.15 wt %) occurred with high S contents (1620 ppm) at the lowermost lower kaolin zone sample ("AND615") where alunite was not detected. These K_2O concentrations may have reflected small amounts of muscovite which were identified per mineralogical analyses for sample AND615 (Fig. S2).

3.3. Whole rock composition: Non-REE trace elements

The non-REE trace elements consisting of Zr, S, Sr, C and Pb showed observable differences throughout this section (Table 4, Table S3, Fig. S4). The enrichments in Zr correlated with gibbsite content, CIA values, and TiO_2 concentrations (Table 2, Fig. 4). Strong correlation between S and Sr concentrations was observed within the upper kaolin zone (Pearson $r = 0.70$). The Sr concentrations in this zone were 10–40 times greater than all other zones (Fig. S4). Concentrations of S were most elevated in the upper kaolin zone with little correlation to Fe (Pearson $r = -0.36$). However, elevated concentrations of S in the lower kaolin zone also showed strong correlation to Fe (Pearson $r = 0.99$).

The elevated S in the lower kaolin zone corresponded with the high organic content in sample AND615. This sample represented the base of the lower kaolin zone and the organic-rich lignite clay. This basal horizon contained the highest overall C (~1.1 wt%; Table 4). These contents were ~10 times greater than those measured from all other samples and zones from the section. The concentration of Pb was notably elevated at this horizon, and enriched >20 times compared to UCC (Table S3).

3.4. Whole rock composition: REE

The total REE content (ΣREE, Table 5, Table S4) ranged from 85 to 458 ppm. REE are commonly known to occur within kaolin-rich strata associated with phosphate minerals, and were compared with P_2O_5 contents in these rocks. The REE did not show correlation within the bauxite and lower kaolin zones (Pearson $r = -0.32$). However, correlation was noted between REE contents and P_2O_5 in the upper kaolin zone (Pearson $r = 0.89$). The P_2O_5 contents in the bauxite and lower kaolin zones varied little, while the REE increased significantly (Fig. 5). Ce concentrations were overall greatest for the LREE (Table 5, Fig. 5). Y and Sc concentrations were overall greater than ΣTb-Lu. Comparison between the LREE and HREE concentrations showed several differences, particularly within the bauxite zone.

The REE concentrations were normalized to show enrichments and depletion relative to average Upper Continental Crust (UCC). The UCC-normalized LREE and HREE concentrations remained relatively consistent with increasing depth in the upper kaolin zone (~0.8–1.3 times UCC). The REE were not fractionated within the upper kaolin zone, as observed by $La/Yb_N = 1.5$ (UCC-normalized values) and $Ce/Ce^* = 1.0$ (Figs. 6 and 7). The lower kaolin zone also showed relatively near-equal LREE and HREE concentrations (~0.6–1.4 times UCC) with minimally fractionated REE ($La/Yb_N = 1.1$, $Ce/Ce^* = 0.8$). However, the bauxite zone showed strong depletion in LREE (<40% UCC, Figs. 6 and 7). Comparatively, HREE remained relatively consistent with depth throughout the section. The values for La/Yb_N ranging from 0.2 to 0.3, and Ce/Ce^* values ranging from 1.3 to 0.8 for the top and bottom portions of the bauxite zone, respectively, showed the notable change differences between LREE and HREE concentrations within the bauxite zone (Fig. 6).

Table 3
Whole rock chemical analyses, major/minor oxides (values in wt%).

ID	Na_2O	MgO	Al_2O_3	SiO_2	P_2O_5	K_2O	CaO	TiO_2	MnO	Fe_2O_3	LOI	Total
AND 605	0.04 ± 0.01	0.05 ± <0.01	37.68 ± 0.09	45.08 ± 0.05	0.09 ± <0.01	0.19 ± <0.01	0.05 ± <0.01	1.30 ± 0.02	0.01 ± <0.01	1.08 ± <0.01	14.19 ± <0.01	99.75 ± 0.01
AND 606	0.05 ± <0.01	0.03 ± <0.01	42.12 ± 0.28	35.86 ± 0.58	0.14 ± 0.02	0.10 ± <0.01	0.04 ± <0.01	1.77 ± 0.05	0.01 ± <0.01	0.93 ± 0.01	18.02 ± 0.66	99.03 ± 0.28
AND 607	0.06 ± 0.02	0.02 ± 0.01	47.76 ± 0.08	27.87 ± 0.05	0.11 ± <0.01	0.10 ± <0.01	0.06 ± <0.01	2.05 ± <0.01	0.01 ± <0.01	0.64 ± <0.01	20.95 ± <0.01	99.60 ± <0.01
AND 608	0.03 ± 0.01	0.02 ± 0.01	47.72 ± 0.03	28.36 ± <0.01	0.06 ± <0.01	0.04 ± <0.01	0.05 ± <0.01	2.03 ± 0.06	0.01 ± <0.01	0.55 ± <0.01	21.02 ± <0.01	99.86 ± <0.01
AND 609	0.02 ± <0.01	0.03 ± <0.01	55.52 ± 0.28	11.60 ± 0.24	0.12 ± <0.01	0.01 ± <0.01	0.03 ± <0.01	2.52 ± 0.16	0.01 ± <0.01	0.41 ± <0.01	28.87 ± 0.19	99.09 ± 0.47
AND 610	0.04 ± 0.01	0.03 ± 0.01	47.62 ± 0.15	28.16 ± 0.06	0.06 ± <0.01	0.02 ± <0.01	0.06 ± <0.01	2.19 ± 0.05	0.01 ± <0.01	0.58 ± <0.01	21.15 ± <0.01	99.90 ± 0.02
AND 617	0.03 ± 0.01	0.04 ± <0.01	48.34 ± 0.18	26.26 ± 0.19	0.06 ± <0.01	0.02 ± <0.01	0.04 ± 0.01	1.96 ± 0.09	0.01 ± <0.01	0.61 ± <0.01	22.2 ± 0.28	99.54 ± 0.21
AND 611	<0.02 ± <0.01	0.02 ± 0.01	45.28 ± 0.05	32.55 ± 0.08	0.05 ± <0.01	0.02 ± <0.01	0.06 ± <0.01	1.96 ± 0.02	0.01 ± <0.01	0.70 ± 0.01	19.2 ± <0.01	99.84 ± <0.01
AND 612	0.04 ± 0.01	0.05 ± <0.01	39.48 ± 0.12	42.61 ± 0.53	0.04 ± 0.01	0.02 ± <0.01	0.04 ± <0.01	1.69 ± 0.05	0.01 ± <0.01	0.64 ± <0.01	15.06 ± 0.47	99.64 ± 0.23
AND 613	0.02 ± <0.01	0.06 ± 0.01	38.46 ± 0.07	45.62 ± 0.04	0.04 ± <0.01	0.04 ± <0.01	0.05 ± <0.01	1.78 ± 0.01	0.01 ± <0.01	0.62 ± 0.01	13.25 ± <0.01	99.92 ± 0.01
AND 614	0.04 ± 0.01	0.06 ± <0.01	37.75 ± 0.06	45.86 ± 0.08	0.05 ± <0.01	0.07 ± <0.01	0.07 ± <0.01	1.57 ± 0.01	0.01 ± <0.01	0.98 ± <0.01	13.37 ± <0.01	99.81 ± 0.01
AND 615	0.04 ± <0.01	0.10 ± <0.01	36.51 ± 0.18	43.66 ± 0.37	0.05 ± 0.01	0.15 ± <0.01	0.08 ± <0.01	1.69 ± 0.03	0.01 ± <0.01	1.05 ± 0.01	15.85 ± 0.22	99.18 ± 0.37

Table 4
Whole rock chemical analyses, non-REE trace elements (values in ppm).

ID	V	Sr	Zr	Nb	Ba	Hf	Ta	Pb	Th	U	C	S
AND 605	219	64.5	40	22.5	117.5 ± 5.3	1	2	29	16	4	1100	1730
	± 0.7	± 0.4	± <0.1	± 0.4		± <0.1	± <0.1	± <0.1	± <0.1	± <0.1	± 49.5	± 28.3
AND 606	273	226	160	29	91.0 ± 0.7	5.7	2.1	26	29.6	12.6	1430	4540
	± 7.8	± 4.9	± 14.5	± 1.4		± 0.2	± 0.1	± <0.1	± 0.4	± 0.4	± 35.4	± 49.5
AND 607	255	293	150	31	94 ± <0.1	7	3	23.5	31	10	1785	3175
	± 1.4	± 3.5	± 1.4	±<0.1		± <0.1	± <0.1	± 0.4	± <0.1	± <0.1	± 10.6	± 24.7
AND 608	289	39.5	252	31	42.5 ± 1.8	6	2	18	28.5	8	1450	985
	± 2.8	± 0.4	± 0.4	± <0.1		± <0.1	± <0.1	± <.10	± 0.4	± <0.1	± 7.1	± 10.6
AND 609	231	11	435	40	17.5 ± 2.5	11.2	2.8	9	36.4	12.9	2300	1140
	± 9.9	± <0.1	± 13.1	± <0.1		± 0.1	± 0.1	± 0.7	± 0.3	± 0.1	± 49.5	± 14.1
AND 610	318	14.5	215	35	26.5 ± 1.1	4.5	3	13	23.5	7.5	1260	470
	± 2.5	± 0.4	± 3.2	± <0.1		± 0.4	± <0.1	± <0.1	± 0.4	± 0.4	± 14.1	± <0.1
AND 617	268	11	210	31	13.5 ± 5.3	4.6	2	8.5	20.8	9.5	1535	1000
	± 10.3	± <0.1	± 4.2	± 0.7		± 0.4	± <0.1	± 0.4	± 1.6	± 0.4	± 24.7	± 7.1
AND 611	265	7	169	28	18.0 ± 0.7	3	2	11	21	12.5	1585	1095
	± 4.2	±<0.1	± 2.1	± 0.7		± <0.1	± <0.1	± <0.1	± 0.7	± 0.4	± 10.6	± 3.5
AND 612	138	11.5	168	27.5	19.0 ± 2.1	3.4	2	10.5	20.7	5.1	990	95
	± 0.4	± 0.4	± 4.6	± 0.4		± 1	± <0.1	± 0.4	± 0.2	± 0.1	± 42.4	± 3.5
AND 613	128	10	173	31.5	37.0 ± 2.8	3	2	19	24	9.5	600	235
	± 3.9	± <0.1	± 1.4	± 0.4		± <0.1	± <0.1	± <0.1	± <0.1	± 0.4	± 14.1	± 3.5
AND 614	162	13	129	26.5	45.5 ± 0.4	2	2	21	19	4	705	1335
	± 2.1	± <0.1	± 1.1	± 0.4		± <0.1	± <0.1	± 0.7	± <0.1	± <0.1	± 24.7	± 10.6
AND 615	166	17	217	26	80.5 ± 6.0	4.2	2.1	586	21.6	16.1	10,730	1625
	± 6.4	± <0.1	± 0.7	± 1.4		± 1.5	± <0.1	± 5.3	± 1.0	± 0.7	± 148	± 3.5

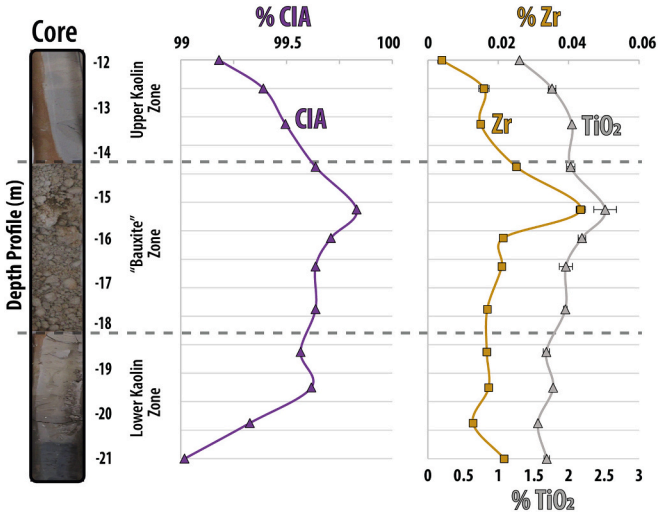

Fig. 4. CIA values (left panel), TiO_2 and Zr (right panel); standard error bars were generally smaller than the symbols employed.

3.5. Ion-exchange extraction: Solid phase residues

The concentrations of the REE were lower for the solid residues after ion exchange, relative to their initial whole rock concentration. Conversely, the concentrations of Mg were higher in the solid residues after ion exchange (Tables 5 and 7, Table S4 and S5; Eq. 3). The increased Mg content in the solid residues after ion-exchange is due to the sorption of Mg onto the kaolinite mineral surfaces. The amount of Mg uptake was determined by subtraction of the Mg content in whole rock starting material from the Mg content of the solid phase residue following ion-exchange (Table 6). Mg uptake (60–416 mg/kg) varied sympathetically with % exchangeable (aq) REE contents in the upper kaolin zone and the top portion of the bauxite zone (Fig. S5). The % exchangeable REE and Mg uptake (229–823 mg/kg) varied antithetically throughout the bottom portion of the bauxite zone and the lower kaolin zone. Overall, Mg uptake showed the strongest correlation with overall kaolinite content across all zones of this section (Pearson r = 0.87).

The % exchangeable (Eq. 3) for the solid residues (s) and the leaching efficiency (Eq. 4) for the ion-exchange leachates (aq) were compared (Fig. S6). This comparison showed consistent trends, particularly for the HREE. The LREE were with less strong consistency and differences ranged ~1–8%, particularly for bauxite zone samples (Fig. S6).

3.6. Chemical analyses from ion-exchange leachates

The analysis of the ion-exchange leachates showed a comparable ion-exchange behavior for all LREE with the exception of Ce (Fig. 8, Table 6, Table 8, Table S6). Ce was markedly lower than ΣLa-Gd (excluding Ce) within the bauxite zone. The % exchangeable content of Ce was 0.2–0.6% whereas the ΣLa-Gd (excl. Ce) ranged from 3.3 to 4.2% at the top portion of the bauxite zone (Table 6). The Ce/LREE values quantified the % exchangeable contents difference between Ce and ΣLa-Gd (excl. Ce). Ce/LREE values were on average 0.7 and 0.8 in the upper kaolin zone and lower kaolin zone, respectively. However, the Ce/LREE values were on average 0.1 and 0.4 for the top and bottom portions of the bauxite zone, respectively. Results for the HREE and ΣTb-Lu were compared with Sc and Y. The small difference in ion-exchangeability trends were evident across the section for ΣTb-Lu and Y. Sc contents showed drastically different results with ion-exchangeability (<3%) compared to all other HREE (3–40%) across the section.

3.7. Chemical analysis from sequential extraction leachates

The sequential extraction experiments yielded three stages of leachates (Table 9, Table 10, Table S7). The Stage 1 extractions (extraction of REE in acid-soluble phases) showed comparable % leachable REE as with % ion-exchangeable values for ΣTb-Lu and Y (Tables 9 and 6, respectively). This similarity was likely due to the Na ion (from sodium acetate reagent, Stage 1 extraction solution) performing a similar desorption reaction as the Mg ion (from magnesium sulfate reagent, ion-exchange solution).

The Stage 1 extraction results were summarized as follows. Firstly, general trends for increasing leachability in LREE and HREE (except Sc) were noted with highest overall values, observed at the base of the lower kaolin zone (Table 9). Secondly, the Stage 1 extractions showed non-soluble (<3% leachable) characteristics for Ce throughout the bauxite zone. Thirdly, the Sc showed low-solubility (<4% acid-soluble REE contents) across the entire section.

Table 5
Whole rock chemical analyses, REE and Mg (values in ppm).

ID	La	Ce	Pr	Nd	Sm	Eu	Gd	Tb	Dy	Ho	Er	Tm	Yb	Lu	Sc	Y	ΣREE	LREE	LREE (w/o Ce)	HREE	ΣTb-Lu	Mg
AND 605	32 ± 1.4	48.5 ± 1.1	7 ± <0.1	13.5 ± 0.4	5 ± <0.1	1 ± <0.1	1.5 ± 0.4	1 ± <0.1	1.5 ± 0.4	1 ± <0.1	1 ± <0.1	<1 ± <0.1	1.5 ± 0.4	<1 ± <0.1	28.5 ± 0.4	8 ± <0.1	151 ± 0.7	109 ± 1.1	60 ± 2.1	42.5 ± 0.4	6 ± <0.1	353 ± 2.1
AND 606	46.2 ± 0.8	94.9 ± 2.0	11.9 ± 1.5	27.4 ± 0.3	5.7 ± 1.7	1.4 ± 0.5	2.6 ± 0.3	0.7 ± 0.2	2 ± <0.1	0.7 ± 0.2	3.1 ± 1.4	0.6 ± 0.3	1.6 ± 0.3	0.6 ± 0.3	30.5 ± 1.1	9.5 ± 0.4	238 ± 4.2	190 ± 0.8	95 ± 2.9	48.1 ± 3.5	8.1 ± 2.1	199 ± 12.7
AND 607	28.5 ± 2.5	84.5 ± 1.8	10.5 ± 1.1	32 ± 1.4	6.5 ± 0.4	1.5 ± 0.4	4 ± <0.1	1 ± <0.1	4 ± 0.7	1 ± <0.1	6 ± <0.1	1 ± <0.1	1.5 ± 0.4	1 ± <0.1	35 ± <0.1	11.5 ± 0.4	228 ± 3.9	168 ± 3.9	83 ± 2.1	60 ±<0.1	13.5 ± 0.4	187 ± 8.5
AND 608	11.5 ± 1.1	22.5 ± 0.4	2 ± <0.1	9.5 ± 0.4	3 ± <0.1	1 ± <0.1	1.5 ± 0.4	1 ± <0.1	3 ± <0.1	1 ± <0.1	1 ± <0.1	1 ± <0.1	2 ± <0.1	1 ± <0.1	28.5 ± 0.4	15 ± <0.1	101 ± 1.4	51 ± 1.4	28.5 ± 1.1	51.5 ± 0.4	8 ± <0.1	208 ± 6.4
AND 609	3.3 ± 1.9	11.3 ± 1.2	1.1 ± 0.1	6.3 ± 0.5	1.5 ± 0.3	0.8 ± 0.2	2.8 ± 0.2	0.8 ± 0.2	3.3 ± 0.2	0.9 ± 0.1	2.2 ± 0.1	0.7 ± 0.2	2.8 ± 0.1	0.7 ± 0.2	28.5 ± 1.8	22 ± <0.1	85.5 ± 0.4	26.9 ± 0.1	15.6 ± 1.1	60.3 ± 1.2	9.8 ± 0.6	166 ± 10.6
AND 610	7.5 ± 1.1	22.5 ± 0.4	4 ± <0.1	10 ± 0.7	3 ± 0.7	1 ± <0.1	1.5 ± 0.4	<1 ± <0.1	3 ± 0.7	1 ± <0.1	1 ± <0.1	<1 ± <0.1	1.5 ± 0.4	<1 ± <0.1	26 ± <0.1	14.5 ± 0.4	96 ± 0.7	49.5 ± 0.4	27 ± 0.1	48 ± 0.7	7.5 ± 0.4	208 ± 2.1
AND 617	8.9 ± 1.3	16.1 ± 1.4	3.6 ± 1.0	8.2 ± 0.1	1.9 ± 0.1	0.7 ± 0.2	1.4 ± 0.2	0.7 ± 0.2	2.1 ± 0.1	0.8 ± 0.2	1.3 ± 0.2	0.6 ± 0.3	1.7 ± 0.2	0.6 ± 0.3	29 ± 1.4	17 ± <0.1	92.5 ± 1.1	40.6 ± 1.8	24.6 ± 0.4	52.7 ± 1.7	6.7 ± 0.2	196 ± 10.6
AND 611	10 ± 2.8	11 ± 1.4	1 ± <0.1	6 ± <0.1	1.5 ± 0.4	<1 ± <0.1	2 ± 0.7	1 ± <0.1	2 ± 0.7	1 ± <0.1	<1 ± <0.1	<1 ± <0.1	4 ± 0.7	<1 ± <0.1	31 ± 0.7	26.5 ± 0.4	95.5 ± 3.2	32.5 ± 3.9	21.5 ± 2.5	65 ± 1.4	7.5 ± 0.4	241 ± 4.2
AND 612	32.8 ± 0.2	37.6 ± 6.1	4.1 ± 0.1	11.7 ± 1.2	3.6 ± 1.0	0.8 ± 0.2	1.6 ± 0.4	0.7 ± 0.2	3 ± 0.1	0.8 ± 0.1	1.5 ± 0.4	0.7 ± 0.2	2 ± <0.1	0.7 ± 0.2	29 ± 0.7	16 ± <0.1	145 ± 6.7	92.1 ± 6.4	54.5 ± 0.4	53.3 ± 0.5	8.3 ± 0.2	296 ± 4.6
AND 613	43.5 ± 0.4	54 ± 1.4	8.5 ± 0.4	13.5 ± 1.8	5 ± <0.1	1 ± <0.1	2 ± 0.7	1 ± <0.1	3 ± <0.1	1 ± <0.1	<1 ± <0.1	<1 ± <0.1	2 ± <0.1	<1 ± <0.1	47.5 ± 0.4	16 ± <0.1	198 ± 2.1	128 ± 2.5	73.5 ± 1.1	70.5 ± 0.4	7 ± <0.1	302 ± 4.2
AND 614	47 ± 0.7	55.5 ± 0.4	7.5 ± 1.1	14 ± 1.4	5 ± <0.1	1 ± <0.1	1.5 ± 0.4	1 ± <0.1	1.5 ± 0.4	1 ± <0.1	<1 ± <0.1	<1 ± <0.1	2.5 ± 0.4	<1 ± <0.1	44.5 ± 0.4	12.5 ± 0.4	194 ± 1.4	132 ± 0.4	76 ± 0.7	63 ± 0.7	6 ± <0.1	359 ± 2.1
AND 615	70.4 ± 0.3	128 ± 60	15.6 ± 0.4	64.7 ± 1.0	12.1 ± 1.4	2.6 ± 0.4	10.8 ± 0.6	1.5 ± 0.3	10.6 ± 1.1	2.7 ± 0.2	3.5 ± 2.5	1.1 ± 0.1	7.8 ± 0.2	1.1 ± 0.1	70 ± 2.1	56 ± 0.7	458 ± 8.8	304 ± 8.2	176 ± 2.2	154 ± 0.8	28.1 ± 3.6	555 ± 33.9

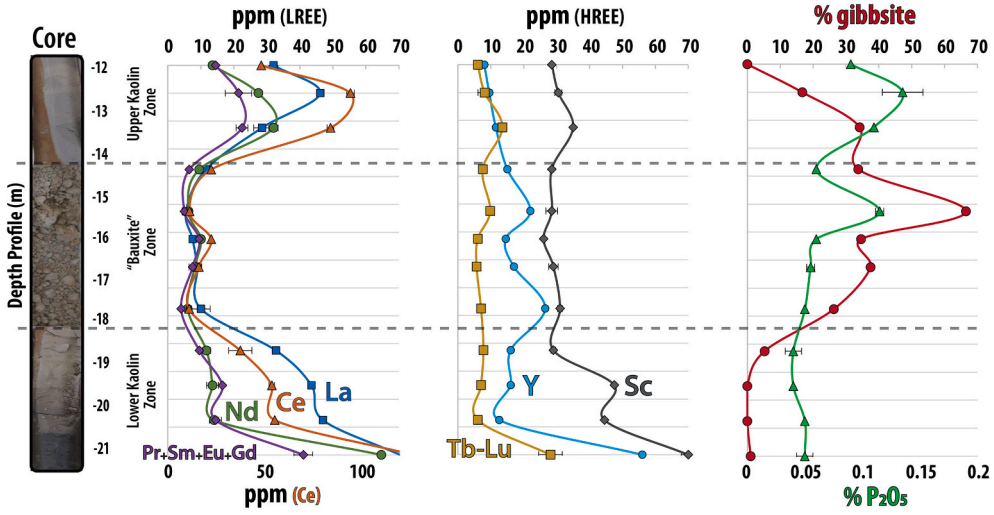

Fig. 5. Absolute concentrations (ppm) for LREE (left panel), HREE (middle panel), P_2O_5 and gibbsite (%; right panel); standard error bars were generally smaller than the symbols employed.

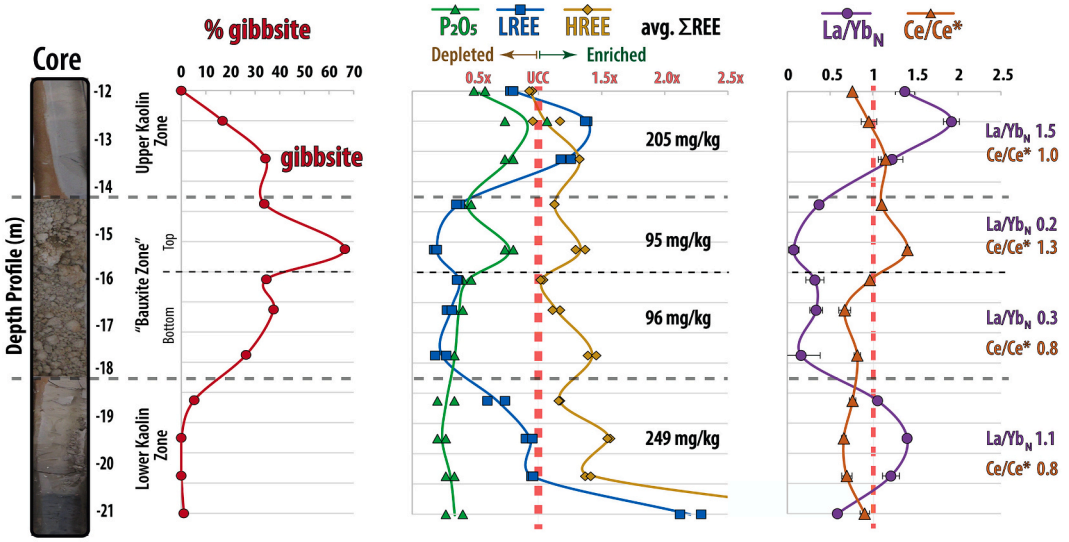

Fig. 6. Gibbsite content (%; left panel); UCC normalized P_2O_5, LREE & HREE values with average ΣREE contents (middle panel); La/Yb_N and Ce/Ce* values (right panel); symbols for duplicate analyses shown (middle panel), standard error bars were generally smaller than the symbols employed (right panel).

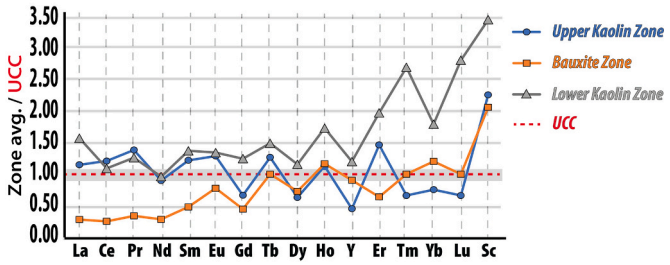

Fig. 7. Diagram showing the REE enrichment and depletion patterns for each zone of the section. The values shown for each REE were calculated from average whole rock REE compositions per zone, normalized to UCC values. Enrichments are represented by values >1, and depletions by values <1. Values for Y were shown following Ho values due to similar ionic radius.

The Stage 2 extractions (reducible phases) showed similar trends for the HREE (ΣTb-Lu + Y). All REE (except Ce, Sc) showed greatest Stage 2 leachability within the bauxite zone and at the base of the lower kaolin zone. Stage 2 leachability was greatest overall for the HREE, with ΣTb-Lu (3–13%), Y (5–17%) and Sc (11–24%). These HREE were more leachable than the LREE. The LREE showed low values (generally <5%), with the exception of the top portion of bauxite zone (9.9%, Table 9). The most conspicuous results for the Stage 2 extractions were the very high leachability values for Sc throughout the section, as compared to its very low leachability during Stage 1 and Stage 3 extractions. The leachability for Sc was strongly consistent with the leachability for Fe (Table 10).

Stage 3 extractions (oxidizable phases) were negligible (<2%) across all samples except the base of the lower kaolin zone. Stage 3 leachability in the lower kaolin zone sample ("AND615") was <5% for LREE and Ce, 9–10% for ΣTb-Lu and Y, and ~15% for Sc (Table 9, Fig. 9). Overall, the base of the lower kaolin zone shows the greatest total extractable REE. The results for the base of the lower kaolin zone occurred with the highest overall C contents. This lowermost sample was a dark, organic-rich lignitic clay having the highest overall C (~1.1 wt%).

Table 6
Ion-exchange chemical analyses, solid phase and leachate phase % exchangeable REE (per Eq. 3 and 4, respectively).

		Upper Kaolin Zone			"Bauxite Zone"					Lower Kaolin Zone			
	Sample ID	AND 605	AND 606	AND 607	AND 608	AND 609	AND 610	AND 617	AND 611	AND 612	AND 613	AND 614	AND 615
solid	LREE	1.9	5.4	4.3	0.6	8.3	11.3	13.2	22.5	0.0	3.2	0.0	9.9
	HREE	8.5	2.5	4.4	8.5	4.8	7.1	10.1	18.0	10.1	0.0	1.1	16.1
	Mg uptake (mg/kg)	416	404	323	284	60	229	380	335	567	760	823	588
leachate phase (aq)	LREE	4.0	0.9	0.5	2.5	2.2	2.9	5.7	15.2	3.8	4.3	3.3	11.1
	ΣLa-Gd (excl. Ce)	3.6	1.1	0.8	4.2	3.3	4.5	7.8	16.6	4.4	4.9	3.6	11.8
	Ce	4.6	0.7	0.1	0.2	0.6	1.0	2.5	12.6	2.9	3.6	3.0	10.2
	Ce/LREE	1.3	0.6	0.2	0.1	0.2	0.2	0.3	0.8	0.7	0.7	0.8	0.9
	HREE	7.9	5.5	3.6	7.2	2.1	7.1	8.9	18.5	10.5	4.3	5.4	18.3
	ΣTb-Lu	13.7	8.8	4.1	11.2	3.0	10.0	10.1	29.4	20.3	12.8	13.2	27.5
	Sc	2.6	2.5	0.8	1.1	0.4	0.8	0.9	0.8	0.9	0.8	2.4	2.7
	Y	22.8	12.3	11.6	16.7	3.9	16.8	22.2	36.3	22.9	10.9	12.5	33.1

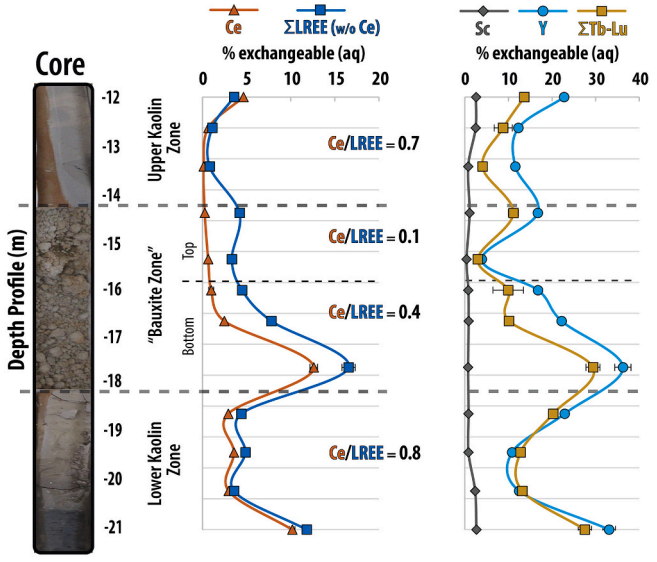

Fig. 8. Ion-exchange leachate (aq) results for Ce versus LREE (excluding Ce; left panel) and ΣTb-Lu versus Y and Sc (right panel); standard error bars were generally smaller than the symbols employed.

4. Discussion

4.1. Upper kaolin zone

The upper kaolin zone did not contain enrichments in the REE. The REE were not depleted nor appreciably fractionated relative to their concentrations in UCC (Fig. 6). The ΣREE contents in the upper kaolin zone (205 ppm) were similar to the total amount of REE in the UCC (183 ppm; Table S4). The absence of REE fractionation was shown by $La/Yb_N = 1.5$ and no Ce/Ce* anomalies. La/Yb_N values >1.0 represented a slight enrichment in the LREE which is not unexpected for clay-rich rocks (Gromet et al., 1984).

LREE enrichments were seen in argillaceous rocks, including shale composite and other clastic sediments (e.g. McLennan and Taylor, 2012; Rudnick and Gao, 2003; Condie, 1991; Gromet et al., 1984; Piper, 1974). The enrichment in the LREE might have occurred during early stages of the weathering of parent rock. For example, the incipient weathering during conversion of volcanic material and volcaniclastic sediments has been shown to yield LREE-enriched, clay-rich rocks (Kadir et al., 2021; Zielinski, 1982). The breakdown of crustal rocks (such as average upper continental crust) resulting in clastic sediments is known to transfer REE such that the sedimentary rocks formed from this crustal protolith are LREE-enriched (e.g. Piper, 1974). Thus, LREE enrichments are not unexpected in the unaltered kaolinitic sediments (Cheshire et al., 2018; Cheshire, 2011).

The possible presence of supergene alunite in the upper kaolin zone samples was conspicuous, as noted per mineralogical and chemical analyses (K_2O, S, Sr). This observation was notable given that minerals of the alunite supergroup (alumino-phosphate-sulfate, APS; Text S6) may contain minor amounts of REE. However, the role of alunite as a REE-bearing phase was apparently insignificant in the upper kaolin zone which showed similar whole rock REE contents to UCC.

4.2. Bauxite zone

The bauxite zone showed ~50% ΣREE relative to UCC concentrations, and thus were depleted in REE compared to the overlying upper kaolin zone (Figs. 6 and 7). These rocks contained sizable depletions in the LREE (<40% LREE relative to UCC contents). Very low La/Yb_N values (0.2) depict the fractionation of LREE and HREE driven by the strong LREE depletion, accompanied by concomitant HREE retention (~1.1–1.3 times UCC contents). Positive Ce/Ce* anomalies (Ce/Ce* = 1.3) were observed at the top portion of the bauxite zone, indicating preferential retention and thus enrichment in Ce relative to the other LREE. Negative Ce/Ce* anomalies of 0.8 were observed for both the bottom portion of the bauxite zone and lower kaolin zone.

The most common occurrence of REE are trivalent charge states. However, Ce can be oxidized to Ce(IV) and mineralized as cerianite (CeO_2; Xu et al., 2017; Bao and Zhao, 2008). CeO_2 is a highly insoluble oxide which will contribute to a positive anomaly where formed, and to a negative anomaly where other REE are deposited elsewhere (Cheshire, 2011). The likelihood of Ce fractionation due to CeO_2 formation was supported by the very low ion-exchangeability for Ce (Ce/LREE = 0.1, Fig. 8). The ion-exchangeable Ce were 0.2–0.6%, whereas all other LREE were 3.3–4.2% within the top portion of the bauxite. It was also supported by the results of the Stage 2 extractions showing a dominantly non-soluble nature of the Ce (0.9–1.2%) compared to all other LREE (4.5–9.9%) in the bauxite zone (Fig. 9, Table 9). If Ce were not insoluble relative to the other LREE, then comparable ion-exchangeability should have been observed as with other LREE (e.g. Borst et al., 2020). However, this was not the case. Therefore, low Ce/LREE, low leachability, and positive whole rock Ce/Ce* anomalies strongly reflected the fractionation and relative insolubility of Ce in this section.

The characteristics of the REE in these rocks were related to autochthonous deposit formation. The bauxite was formed by in-situ weathering of the older sedimentary kaolin strata. The bauxite zone contained readily observable pisolites and high measurable quantities of gibbsite. The formation of gibbsite was accompanied by elevated concentrations of insoluble elements contents (Ti, Zr), and low concentrations of alkali and alkaline. High CIA values and Al_2O_3:SiO_2 ratios were

Table 7
Ion-exchange chemical analyses, solid phase residues (post-ion-exchange; values in ppm).

ID	La	Ce	Pr	Nd	Sm	Eu	Gd	Tb	Dy	Ho	Er	Tm	Yb	Lu	Sc	Y	ΣREE	LREE	LREE (w/o Ce)	HREE	ΣTb-Lu	Mg
AND 605	30.3 ± 0.7	47.7 ± 0.3	6.7 ± 0.3	12.3 ± 0.3	4.3 ± 0.5	1 ± <0.1	2.7 ± 0.3	1 ± <0.1	2.3 ± 0.3	1 ± <0.1	1 ± <0.1	<1 ± <0.1	1 ± <0.1	<1 ± <0.1	28 ± 0.5	6 ± <0.1	144.3 ± 0.7	105 ± 0.9	57.3 ± 0.7	39.3 ± 0.3	5.3 ± 0.3	756 ± 10.7
AND 606	40.7 ± 1.4	91.3 ± 1.1	10 ± <0.1	26.3 ± 0.3	8 ± <0.1	1 ± <0.1	3.3 ± 0.3	1 ± <0.1	2.7 ± 0.3	1 ± <0.1	5 ± <0.1	<1 ± <0.1	1 ± <0.1	<1 ± <0.1	32 ± 0.5	9 ± <0.1	232.3 ± 0.5	181 ± 1.0	89.3 ± 1.7	51.7 ± 0.7	10.7 ± 0.3	593 ± 8.6
AND 607	24.3 ± 3.5	78.7 ± 1.0	9.3 ± 1.0	30.7 ± 1.0	6.3 ± 0.3	1 ± <0.1	4.7 ± 0.3	1 ± <0.1	2.7 ± 0.3	1 ± <0.1	6 ± <0.1	<1 ± <0.1	1.3 ± 0.3	<1 ± <0.1	35.3 ± 0.5	10 ± <0.1	212.3 ± 1.8	155 ± 2.4	76.3 ± 1.8	57.3 ± 1.0	12.0 ± 0.5	505 ± 4.3
AND 608	12.3 ± 1.2	22.7 ± 0.7	3 ± 0.5	9.7 ± 0.3	2.3 ± 0.3	1 ± <0.1	1 ± <0.1	1 ± <0.1	2 ± 0.5	1 ± <0.1	1 ± <0.1	<1 ± <0.1	1.3 ± 0.3	<1 ± <0.1	28.3 ± 0.3	12 ± <0.1	98.3 ± 1.8	51.7 ± 1.5	29.0 ± 1.9	46.7 ± 0.3	6.3 ± 0.3	485 ± 6.2
AND 609	<1 ± <0.1	12 ± 0.9	1.5 ± 0.3	7 ± 0.5	0.3 ± 0.3	<1 ± <0.1	1.7 ± 0.5	1 ± <0.1	2 ± 0.5	1 ± <0.1	1.7 ± 0.3	<1 ± <0.1	3 ± <0.1	<1 ± <0.1	30 ± <0.1	21 ± <0.1	81 ± 0.5	22.0 ± 0.5	10.0 ± 1.2	59.0 ± 0.5	8.0 ± 0.5	225 ± 1.6
AND 610	6 ± 1.2	22 ± 0.9	3 ± 0.5	8.7 ± 0.3	1.7 ± 0.3	1 ± <0.1	2 ± <0.1	1 ± <0.1	1 ± <0.1	1 ± <0.1	1 ± <0.1	<1 ± <0.1	2 ± <0.1	<1 ± <0.1	26.7 ± 0.3	11.7 ± 0.3	88 ± 0.5	44.3 ± 0.7	22.3 ± 1.4	43.7 ± 0.5	5.3 ± 0.3	430 ± 5.9
AND 617	7.3 ± 1.2	14 ± 0.9	3 ± 0.8	7.7 ± 1.4	1.7 ± 0.3	1 ± <0.1	1.5 ± 0.5	0.5 ± 0.3	1.7 ± 0.3	1 ± <0.1	<1 ± <0.1	<1 ± <0.1	2 ± <0.1	<1 ± <0.1	29.7 ± 0.5	13 ± <0.1	80.7 ± 0.7	33.0 ± 0.9	19.0 ± 0.1	47.7 ± 1.0	5.0 ± 0.5	571 ± 5.9
AND 611	8.3 ± 2.0	11.7 ± 0.5	1.7 ± 0.3	4.3 ± 0.7	1.3 ± 0.3	<1 ± <0.1	1.3 ± 0.3	0.7 ± 0.3	1.7 ± 0.3	1 ± <0.1	<1 ± <0.1	<1 ± <0.1	2 ± <0.1	<1 ± <0.1	31 ± <0.1	15.3 ± 0.3	80.3 ± 1.4	28.7 ± 1.5	17.0 ± 1.4	51.7 ± 0.3	5.3 ± 0.3	573 ± 4.9
AND 612	31.7 ± 2.3	30 ± 1.9	4.7 ± 0.5	11 ± 0.5	3.7 ± 0.3	1 ± <0.1	2.5 ± 0.7	1 ± <0.1	2 ± <0.1	1 ± <0.1	<1 ± <0.1	<1 ± <0.1	2 ± <0.1	<1 ± <0.1	30 ± <0.1	12 ± <0.1	131.3 ± 1.8	83.7 ± 1.5	53.7 ± 0.7	47.7 ± 0.3	5.7 ± 0.3	848 ± 25.6
AND 613	40.3 ± 0.3	50.7 ± 1.7	8 ± 0.5	14 ± 0.5	4.7 ± 0.3	1 ± <0.1	1.3 ± 0.3	0.7 ± 0.3	3.3 ± 0.3	1 ± <0.1	<1 ± <0.1	<1 ± <0.1	2.3 ± 0.3	<1 ± <0.1	48.7 ± 0.3	15 ± <0.1	191 ± 1.7	120 ± 2.1	69.3 ± 0.7	71.0 ± 0.5	7.3 ± 0.3	1043 ± 18.8
AND 614	53 ± 1.2	52 ± 0.5	8.7 ± 0.7	13 ± 0.5	5.3 ± 0.3	1 ± <0.1	0.5 ± 0.3	1 ± <0.1	2.3 ± 0.5	1 ± <0.1	<1 ± <0.1	<1 ± <0.1	1 ± <0.1	<1 ± <0.1	45 ± 0.5	11. ± 0.3	194.7 ± 1.1	133 ± 1.4	81.3 ± 1.4	61.3 ± 0.3	4.7 ± 0.7	1156 ± 22.9
AND 615	60.7 ± 1.8	107.3 ± 2.8	16 ± <0.1	60.3 ± 1.0	9.7 ± 0.3	2 ± <0.1	7 ± 0.5	1 ± <0.1	7.3 ± 0.3	2 ± <0.1	1 ± <0.1	1 ± <0.1	5 ± <0.1	<1 ± <0.1	75 ± 0.5	36.3 ± 0.3	391.3 ± 2.9	263 ± 2.1	155.7 ± 0.7	128 ± 1.0	17 ± 0.5	1132 ± 20.5

Table 8
Ion-exchange chemical analyses, leachate (aq; values in ppb).

ID	La	Ce	Pr	Nd	Sm	Eu	Gd	Tb	Dy	Ho	Er	Tm	Yb	Lu	Sc	Y	ΣREE	LREE	LREE (w/o Ce)	HREE	ΣTb-Lu
AND 605	7.3 ± 0.04	56.2 ± 0.95	4.5 ± 0.04	24.9 ± 0.11	7.0 ± 0.07	1.6 ± 0.04	8.5 ± 0.07	1.4 ± 0.04	7.9 ± 0.42	1.6 ± 0.07	4.5 ± 0.18	0.7 ± 0.04	3.9 ± 0.21	0.7 ± 0.04	18.4 ± 0.42	45.6 ± 0.21	195 ± 1.06	110 ± 0.74	53.7 ± 0.23	84.4 ± 1.64	20.5 ± 0.99
AND 606	2.8 ± 0.35	15.8 ± 1.06	1.9 ± 0.11	11.2 ± 0.64	4.1 ± 0.18	1.1 ± 0.04	5.5 ± 0.21	0.9 ± 0.07	5.3 ± 0.35	1.1 ± 0.04	2.8 ± 0.18	0.4 ± 0.04	7.1 ± 3.50	0.4 ± 0.04	19.0 ± 1.13	29.2 ± 1.06	108 ± 9.19	42.1 ± 2.62	26.3 ± 1.58	66.1 ± 6.36	17.8 ± 4.18
AND 607	0.7 ± 0.11	2.7 ± 0.25	0.6 ± 0.04	6.1 ± 0.46	3.2 ± 0.11	1.0 ± 0.04	5.4 ± 0.14	0.9 ± 0.04	5.0 ± 0.32	1.0 ± 0.07	2.7 ± 0.14	0.4 ± 0.04	3.5 ± 1.10	0.4 ± 0.04	6.9 ± 1.24	33.4 ± 0.92	73.0 ± 4.95	19.4 ± 1.16	16.8 ± 0.89	53.9 ± 3.85	13.7 ± 1.7
AND 608	0.4 ± 0.14	1.4 ± 0.35	0.7 ± 0.07	11.4 ± 0.53	5.9 ± 0.28	1.7 ± 0.11	9.8 ± 0.32	1.5 ± 0.11	8.4 ± 0.49	1.8 ± 0.11	4.6 ± 0.25	0.7 ± 0.04	5.0 ± 1.27	0.6 ± 0.04	7.9 ± 1.31	62.8 ± 2.02	125 ± 7.42	31.4 ± 1.87	30.0 ± 1.53	92.9 ± 5.57	22.3 ± 2.25
AND 609	0.6 ± 0.11	1.8 ± 0.28	0.6 ± 0.04	5.7 ± 0.42	2.2 ± 0.14	0.6 ± <0.01	3.3 ± 0.11	0.5 ± <0.01	2.4 ± 0.14	0.6 ± 0.04	1.3 ± 0.04	0.2 ± <0.01	2.3 ± 1.06	0.2 ± <0.01	3.0 ± 1.1	21.4 ± 0.88	46.5 ± 4.6	14.7 ± 1.06	13.0 ± 0.80	31.7 ± 3.25	7.3 ± 1.25
AND 610	2.3 ± 0.60	5.6 ± 1.52	1.5 ± 0.18	13.8 ± 1.17	4.6 ± 0.32	1.2 ± 0.07	7.1 ± 0.28	0.9 ± 0.04	4.5 ± 0.32	1.0 ± 0.07	2.4 ± 0.18	0.3 ± <0.01	9.6 ± 5.94	0.2 ± <0.01	5.3 ± 1.48	60.8 ± 2.4	121 ± 14.5	35.8 ± 4.12	30.3 ± 2.58	84.8 ± 10.4	18.7 ± 6.54
AND 617	7.8 ± 0.07	10.0 ± 0.04	2.4 ± <0.01	19.7 ± 0.14	6.6 ± 0.11	1.8 ± 0.07	9.9 ± 0.11	1.3 ± 0.04	7.2 ± 0.32	1.5 ± 0.07	3.9 ± 0.21	0.5 ± 0.04	2.2 ± 0.14	0.3 ± <0.01	6.4 ± 1.31	94.5 ± 0.60	176 ± 3.18	57.9 ± 0.55	48.0 ± 0.51	118 ± 2.75	16.9 ± 0.84
AND 611	19.6 ± 0.78	34.7 ± 1.17	5.7 ± 0.25	33.6 ± 1.73	9.7 ± 0.53	2.9 ± 0.18	17.8 ± 0.60	2.9 ± 0.14	20.2 ± 1.20	5.0 ± 0.25	14.3 ± 0.85	1.8 ± 0.07	9.6 ± 0.49	1.5 ± 0.04	6.0 ± 1.03	241 ± 12.4	425 ± 21.9	124 ± 5.24	89.0 ± 4.07	301 ± 16.5	55.1 ± 2.99
AND 612	14.9 ± 0.21	27.4 ± 0.21	4.3 ± 0.07	23.1 ± 0.60	6.3 ± 0.11	1.8 ± 0.04	9.7 ± 0.07	1.9 ± 0.04	13.7 ± 0.49	3.3 ± 0.07	10.4 ± 0.25	1.5 ± <0.10	9.8 ± 0.25	1.5 ± 0.04	6.3 ± 0.81	92.0 ± 0.39	227 ± 2.83	87.0 ± 1.40	59.9 ± 1.19	140 ± 1.55	41.8 ± 1.15
AND 613	33.4 ± 5.52	48.1 ± 1.17	7.0 ± 0.25	33.5 ± 1.45	7.2 ± 0.32	1.7 ± 0.11	6.9 ± 0.28	1.1 ± 0.07	7.3 ± 0.39	1.6 ± 0.07	5.0 ± 0.25	0.9 ± 0.04	5.9 ± 0.32	0.9 ± 0.04	10.0 ± 0.99	43.0 ± 1.31	214 ± 1.77	137 ± 1.93	89.4 ± 3.12	75.9 ± 3.48	22.4 ± 1.14
AND 614	22.7 ± 0.57	41.2 ± 1.13	5.8 ± 0.18	26.9 ± 1.03	5.8 ± 0.21	1.3 ± 0.07	5.7 ± 0.21	1.0 ± 0.07	6.3 ± 0.42	1.5 ± 0.11	4.5 ± 0.28	0.8 ± 0.04	5.1 ± 0.28	0.8 ± 0.04	26.6 ± 1.52	39 ± 1.2	195 ± 7.42	109 ± 3.45	68.0 ± 2.33	85.3 ± 3.85	19.8 ± 1.15
AND 615	170 ± 4.6	325 ± 9.55	42.0 ± 0.88	198 ± 5.66	47.3 ± 1.38	11.0 ± 0.46	52.2 ± 1.38	8.8 ± 0.42	62.6 ± 3.61	14.4 ± 0.67	45.4 ± 2.33	7.0 ± 0.32	48.3 ± 3.11	7.1 ± 0.32	47.0 ± 1.8	464 ± 20.2	1549 ± 56.9	845 ± 24.2	521 ± 14.7	704 ± 32.7	193 ± 10.7

Table 9
Sequential extraction chemical analyses, leachability (%) per Eq. 4.

	Stage 1 – acid-soluble					Stage 2 – reducible					Stage 3 – oxidizable				
Sample ID	AND 606	AND 609	AND 617	AND 612	AND 615	AND 606	AND 609	AND 617	AND 612	AND 615	AND 606	AND 609	AND 617	AND 612	AND 615
LREE	0.9	3.3	6.6	4.8	9.3	0.4	5.9	3.2	1.8	4.6	0.1	0.5	0.4	0.8	5.0
ΣLa-Gd (excl. Ce)	1.2	5.4	9.4	5.7	10.6	0.5	9.9	4.5	2.1	4.9	0.1	0.8	0.6	0.9	5.0
Ce	0.6	0.5	2.4	3.5	7.6	0.3	0.9	1.2	1.4	4.3	0.0	0.1	0.2	0.7	5.1
HREE	6.0	2.9	6.9	14.1	17.5	11.5	16.8	17.9	8.9	16.9	1.4	1.0	1.1	1.4	12.1
ΣTb-Lu	6.0	3.8	13.5	27.8	28.1	3.2	12.6	12.1	7.1	11.4	0.4	0.9	1.1	2.0	9.9
Sc	4.0	1.0	1.5	1.6	2.9	15.7	20.1	19.6	11.0	23.4	1.9	1.1	1.1	1.2	15.3
Y	12.3	4.9	13.8	30.0	30.4	4.9	14.5	17.0	5.8	11.5	0.6	0.7	1.2	1.6	9.1
Fe	<0.1	<0.1	<0.1	<0.1	0.1	11.7	12.7	11.6	11.5	16.0	5.6	2.3	2.5	0.1	3.9

consistent for highly weathered rocks such as lateritic bauxites (Voicu and Bardoux, 2002; Fedo et al., 1995; Middelburg et al., 1988; Nesbitt and Young, 1982). Dissolution and leaching of mobile constituents (e.g. silica, alkali and alkaline earths) resulted in a residuum further enriched in insoluble constituents (Mamedov et al., 2022; Yang et al., 2022; Lukas et al., 1983; Norton, 1973).

Few studies have conducted similar investigations into the REE characteristics of kaolin-rich sedimentary rocks. Murakami and Ishihara (2008) reported REE contents in sedimentary kaolin deposits derived from weathered granites in the Sanyo belt, Japan, however, these deposits contained no bauxite. Baioumy and Gilg (2011) investigated kaolins with relict "pisoliths" from the Kalabsha region, Egypt, which "unambiguously indicated" transport and deposition of lateritic materials (overlying weathered granites) forming allochthonous deposits. These kaolins with pisoliths and other textures showed Ce anomalies and depletion in LREE, but these rocks did not contain measurable quantities of gibbsite (or other Al-hydroxide minerals; Baioumy and Gilg, 2011). Furthermore, Baioumy and Gilg (2011) reported that the total REE contents were correlated with P_2O_5 contents and REE-bearing phosphate minerals.

REE-bearing phosphate minerals are common trace constituents in the Georgia kaolins, related to the original sediment source input (Boxleiter and Elliott, 2023; Elliott et al., 2018; Cheshire et al., 2018). However, these bauxite-kaolins rocks investigated herein showed no correlation between P_2O_5 and REE concentrations in the bauxite and lower kaolin zones (Fig. 5, Fig. 6). Therefore, the REE abundances in the bauxite zone and lower kaolin zone cannot be explained solely by the presence of REE-bearing phosphate minerals. The results warranted further consideration of the solubilization of the REE, and their sorption/precipitation on mineral surfaces in these strata.

4.3. Lower kaolin

Relatively high percentages of ion-exchangeable REE were found both at the base of the bauxite zone and at the base of the lower kaolin zone where gibbsite mineral contents are ≤5 wt%. The % ion-exchangeable values for LREE (15–17%), ΣTb-Lu (~29%) and Y (~36%) at the base of the bauxite zone were very similar to the % ion-exchangeable values for LREE (11–12%), ΣTb-Lu (~28%) and Y (~33%) at the base of the lower kaolin zone (Fig. 8, Table 6). Although, the ΣREE contents at the base of the bauxite zone were on average 96 ppm (~50% ΣREE contents relative to UCC) and thus cannot be considered enrichment in REE relative to the UCC. The relatively high percentage of ion-exchangeable REE still warranted future investigation.

The accumulation of sorbed and exchangeable REE at the base of the bauxite zone likely resulted likely from the migration of weathering solutions containing dissolved REE. These solutions were conceivably percolating downward from the REE depleted bauxite zone undergoing high degrees of chemical weathering ("bauxitization"). Eventually these fluids encountered the kaolinite-rich strata at the base of the bauxite zone. Some portions of the REE were sorbed onto kaolinite mineral surfaces in the base of the bauxite zone. The other portion of REE remained in solution and continued to migrate through the underlying strata into the lower kaolin zone.

Hypothetically, the soluble REE entering the lower kaolin zone were responsible for the occurrence of significant portions of ion-exchangeable REE present at the base of the lower kaolin zone. The ΣREE contents in the lowermost sample ("AND615") of the lower kaolin zone were ~460 ppm. These ΣREE contents are ~250% relative to UCC and are therefore enriched. The base of the lower kaolin zone with elevated ion-exchangeable content represents a second horizon of ion-sorption clay (IAC) accumulated REE.

The base of the bauxite zone also contained significantly higher extractable REE from the Stage 3 extractions (oxidizable phases and bound REE). All other zones and samples showed negligible Stage 3 extractable REE (<2%; Table 9, Table 10, Fig. 9). Extractable REE within the base of the bauxite zone ranged from ~5% for the LREE and 9–15% for the HREE. Higher extractable HREE contents compared to LREE is expected due to conspicuously high C contents noted per chemical analyses.

These C contents are due to the stratigraphic transition with lignitic clay at the base of this section underlying the lower kaolin zone. The organic carbon content has been observed to influence redox conditions in kaolinite-rich rocks (Cheshire et al., 2012; Taunton et al., 2000). Organic ligands duly play a strong role in REE complexation. These ligands facilitate transport and sorption reactions with mineral surfaces, especially considering the stronger bond between HREE and organic ligands compared to LREE (Sanematsu and Watanabe, 2016; Yusoff et al., 2013; Cheshire et al., 2012; Tang and Johannesson, 2003, 2010; Wan and Liu, 2006; Wood, 1990).

4.4. Scandium

Sc contents did not correlate with whole rock CIA values, gibbsite contents, or other insoluble elements such as Zr and Ti. Likewise, Sc contents showed several prominent differences compared to all other REE. For example, other HREE (ΣTb-Lu and Y) were more exchangeable (3–40% ion-exchangeable). Comparatively, Sc was not exchangeable (<3%) across the entire section. However, the Sc contents showed consistently higher solubility (11–24%) compared to all other REE (1–17%; Fig. 9) under reducing conditions during Stage 2 extractions (reducible phases).

Sc may be incorporated into iron-oxyhydroxides, TiO_2 minerals, and precipitation or adsorption with Fe/Mn/Al-oxides which scavenge the REE/Fe/Mn input from weathering of primary minerals (Brahim et al., 2022; Yan et al., 2019; Li et al., 2019; Yusoff et al., 2013; Bao and Zhao, 2008). TiO_2 minerals (such as anatase, identified per XRD analyses) could incorporate Sc due to similarities in effective ionic radius per coordination state (Shannon, 1976). However, Sc related to TiO_2 minerals was ruled out to explain the Sc contents due to lack of correlation between Sc and TiO_2 whole rock contents. Sc related to adsorption onto clay mineral surface was ruled out due to very low ion-exchangeable Sc contents (<3%) across all samples. The strongest correlation for Sc was found with Fe_2O_3 contents. Consequently, the Stage 2 extractions

Table 10
Sequential extraction chemical analyses, leachates (aq; values in ppb).

	ID	La	Ce	Pr	Nd	Sm	Eu	Gd	Tb	Dy	Ho	Er	Tm	Yb	Lu	Sc	Y	ΣREE	LREE	LREE (w/o Ce)	HREE	ΣTb-Lu	Fe	Mn
	AND 606	2.9 ± 0.07	18.4 ± 0.21	2.3 ± 0.04	14.7 ±0.11	5.7 ± 0.07	1.6 ± 0.04	8.2 ± 0.07	1.3 ± <0.01	7.1 ± <0.01	1.4 ± <0.01	3.6 ± <0.01	0.6 ± 0.04	2.7 ± 0.04	0.5 ± <0.01	37.8 ± 0.28	36.4 ± 0.49	145 ± 1.41	54.0 ± 0.60	35.3 ± 0.39	89.5 ± 2.05	15.3 ± 1.27	22.0 ± 2.12	0.2 ± <0.01
	AND 609	1.0 ± 0.25	1.9 ± 0.04	0.7 ± <0.01	9.3 ±0.04	4.5 ± 0.04	1.4 ± 0.04	7.2 ± <0.01	1.0 ± <0.01	5.0 ± <0.01	1.1 ± 0.04	2.4 ± <0.01	0.4 ± 0.04	1.5 ± <0.01	0.3 ± <0.01	9.3 ± <0.01	33.8 ± 0.11	80.5 ± 0.35	25.8 ± 0.25	23.9 ± 0.21	54.7 ± 0.04	11.6 ± 0.07	<1 ± <0.01	0.4 ± 0.04
Stage 1	AND 617	9.7 ± 0.14	12.2 ± 0.21	3.5 ± 0.32	29.6 ±1.41	10.2 ± 0.18	2.9 ± 0.04	16.2 ± 0.28	2.0 ± 0.04	10.7 ± 0.21	2.3 ± 0.04	5.4 ± 0.14	0.6 ± <0.01	2.6 ± 0.04	0.4 ± <0.01	14 ± 0.07	73.3 ± 15.1	196 ± 18.0	84.0 ± 2.58	72.0 ± 2.37	111 ± 15.6	23.9 ± 0.46	<1 ± <0.01	3.0 ± 0.07
	AND 612	22.1 ± 0.18	40.9 ± 0.28	6.6 ± <0.01	37.2 ±0.07	10.4 ± 0.11	2.9 ± <0.01	16.7 ± 0.21	3.1 ± 0.04	22.8 ± 0.11	5.6 ± 0.04	16.8 ± 0.14	2.4 ± <0.01	14.6 ± 0.14	2.3 ± 0.04	14.5 ± 0.21	150 ± 1.41	369 ± 2.47	137 ± 0.71	95.8 ± 0.42	232 ± 2.12	67.4 ± 0.49	5.0 ± 2.83	5.4 ± 0.07
	AND 615	151 ± 5.66	302 ± 11.7	44.1 ± 1.73	235 ±9.55	62.7 ± 2.69	15.3 ± 0.67	74.6 ± 3.04	12.4 ± 0.85	83.2 ± 3.46	19.4 ± 0.74	58.7 ± 2.26	8.6 ± 0.32	55.9 ± 2.12	8.8 ± 0.32	62.7 ± 3.36	533 ± 21.6	1725 ± 69.7	884 ± 35.0	582 ± 23.3	842 ± 35.0	247 ± 10.1	232 ± 2.83	12.8 ± <0.01
	AND 606	1.3 ± <0.01	7.5 ± 0.11	0.8 ± <0.01	4.9 ±0.07	1.8 ± <0.01	0.5 ± <0.01	2.2 ± 0.04	0.4 ± <0.01	2.4 ± 0.04	0.5 ± 0.04	1.4 ± 0.04	0.2 ± <0.01	1.5 ± 0.04	0.2 ± <0.01	120 ± 4.24	11.7 ± 0.25	157 ± 4.95	19.0 ± 0.21	11.5 ± 0.11	138 ± 4.63	6.4 ± 0.14	19,207 ± 93.3	0.5 ± <0.01
	AND 609	0.4 ± <0.01	2.6 ± 0.07	1.0 ± 0.04	11.9 ±0.35	7.5 ± 0.21	2.2 ± 0.07	12.0 ± 0.39	2.1 ± 0.07	12.5 ± 0.35	2.5 ± 0.07	6.8 ± 0.18	0.9 ± <0.01	5.3 ± 0.14	0.8 ± 0.04	143 ± 6.36	80.0 ± 2.62	292 ± 11.0	38.0 ± 1.13	34.9 ± 1.06	254 ± 9.83	30.8 ± 0.85	9130 ± 183	0.7 ± 0.07
Stage 2	AND 617	2.5 ± 0.07	4.7 ± 0.21	1.5 ± 0.07	11.4 ±0.04	4.4 ± 0.14	1.3 ± 0.04	6.5 ± 0.25	1.1 ± <0.01	6.9 ± 0.18	1.5 ± 0.04	4.1 ± 0.11	0.5 ± <0.01	2.8 ± <0.01	0.4 ± <0.01	142 ± 2.83	72.3 ± 2.72	264 ± 6.72	32.0 ± 0.60	27.5 ± 0.39	231 ± 5.87	17.2 ± 0.32	12,418 ± 355	0.7 ± <0.01
	AND 612	5.3 ± 0.53	13.4 ± 1.24	2.4 ± 0.21	13.2 ±1.17	3.6 ± 0.28	0.9 ± 0.07	3.6 ± 0.28	0.7 ± 0.04	4.5 ± 0.25	1.0 ± 0.07	3.2 ± 0.18	0.6 ± 0.04	3.5 ± 0.21	0.5 ± <0.01	79.9 ± 28.4	23.2 ± 1.52	159 ± 34.7	42.0 ± 3.78	28.9 ± 2.55	116.9 ± 30.7	13.8 ± 0.78	12,651 ± 526	0.8 ± <0.01
	AND 615	50.7 ± 0.07	137 ± 0.35	19.5 ± 0.04	92.4 ±0.18	24.5 ± 0.11	5.4 ± 0.04	22.0 ± 0.04	3.8 ± 0.04	25.5 ± 0.18	5.5 ± 0.04	17.7 ± 0.14	3.0 ± 0.04	21.7 ± 0.14	3.1 ± <0.01	409 ± 2.83	162 ± 0.35	1001 ± 2.12	351 ± 0.04	214 ± 0.32	651 ± 1.91	80.1 ± 0.57	29,118 ± 1096	1.6 ± 0.11
	AND 606	0.5 ± 0.04	1.4 ± 0.04	0.3 ± 0.04	1.7 ±0.11	0.6 ± 0.04	0.1 ± <0.01	0.7 ± 0.04	0.1 ± <0.01	0.6 ± 0.04	0.1 ± <0.01	0.3 ± 0.04	0.1 ± <0.01	0.3 ± 0.04	0.1 ± <0.01	22.3 ± 0.95	2.2 ± 0.04	31.0 ± 0.71	5.0 ± 0.21	3.7 ± 0.25	25.7 ± 0.88	1.3 ± 0.04	1402 ± 268	0.3 ± 0.04
	AND 609	0.2 ± 0.04	0.4 ± < 0.01	0.2 ± <0.01	1.8 ±0.04	0.9 ± 0.04	0.2 ± <0.01	1.2 ± 0.04	0.2 ± <0.01	1.4 ± 0.04	0.3 ± <0.01	0.7 ± <0.01	0.1 ± <0.01	0.7 ± <0.01	0.1 ± <0.01	12.5 ± 0.95	6.2 ± 0.11	27.0 ± 1.41	5.0 ± 0.14	4.3 ± 0.14	22.1 ± 1.1	3.5 ± 0.04	2552 ± 346	0.3 ± <0.01
Stage 3	AND 617	0.7 ± 0.04	1.3 ± 0.04	0.4 ± <0.01	2.8 ±0.21	0.8 ± 0.04	0.2 ± <0.01	0.9 ± 0.04	0.2 ± 0.04	1.0 ± 0.04	0.2 ± <0.01	0.5 ± <0.01	0.1 ± <0.01	0.4 ± <0.01	0.1 ± 0.04	12.5 ± 1.1	8.0 ± 0.25	30.0 ± 1.77	7.0 ± 0.35	5.7 ± 0.32	22.8 ± 1.45	2.4 ± 0.11	4201 ± 174	<1 ± <0.01
	AND 612	5.6 ± 0.07	10.2 ± 0.04	1.7 ± <0.01	8.0 ±0.04	1.7 ± 0.04	0.4 ± <0.01	1.7 ± 0.04	0.3 ± <0.01	1.9 ± <0.01	0.4 ± <0.01	1.3 ± <0.01	0.2 ± <0.01	1.6 ± <0.01	0.2 ± <0.01	12.9 ± 0.28	9.8 ± <0.01	58.0 ± 0.35	29.0 ± <0.01	19.0 ± 0.04	28.6 ± 0.28	5.9 ± <0.01	244 ± 32.2	<1 ± <0.01
	AND 615	113 ± 2.47	253 ± 5.3	32 ± 0.71	131 ±2.83	29.0 ± 0.71	6.3 ± 0.11	25.9 ± 0.6	4.8 ± 0.11	33.7 ± 0.64	7.4 ± 0.14	24.0 ± 0.49	4.1 ± 0.11	29.1 ± 0.46	4.0 ± 0.07	412 ± 3.54	196 ± 5.3	1303 ± 23.3	589 ± 12.7	337 ± 7.42	714 ± 10.9	107 ± 2.02	10,937 ± 73.5	<1 ± <0.01

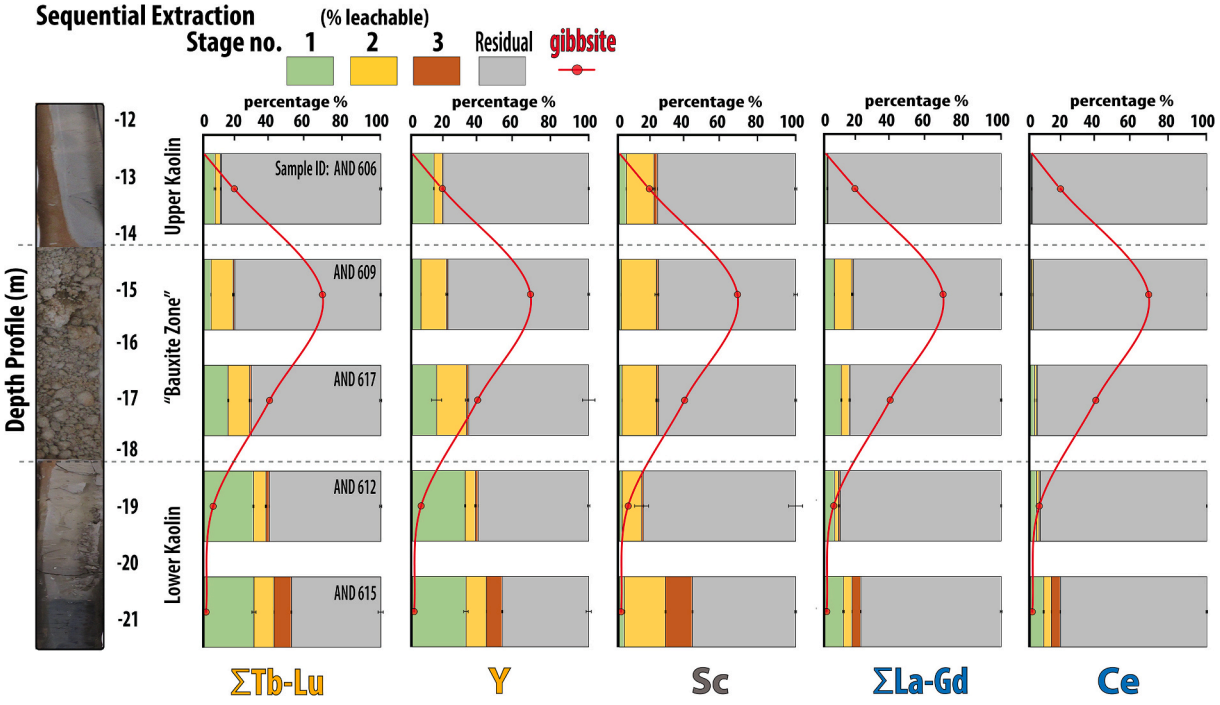

Fig. 9. Stacked bar plot showing sequential extraction leaching efficiency (%) results for ΣTb-Lu, Y, Sc, LREE (excluding Ce), and Ce for select samples in the section.

showed strongly comparable values between Sc and Fe.

Sc and Fe are commonly associated with iron-oxyhydroxide minerals in highly weathered rocks (Text S7; Wang et al., 2021; Chasse et al., 2019). Incorporation into iron-oxyhydroxide minerals was the most likely host for Sc in these rocks due to similar charge and ionic radius for Sc^{3+} and Fe^{3+} (Gamaletsos et al., 2018; Vind et al., 2018; Williams-Jones and Vasyukova, 2018; Mongelli et al., 2017). Sc associations have been previously reported for ore forming processes related to the development of ion-adsorption clay (IAC) deposits (Li et al., 2017, 2019, Li and Zhou, 2020; Sanematsu et al., 2015; Yusoff et al., 2013; Bao and Zhao, 2008; Murakami and Ishihara, 2008; Wu et al., 1990).

4.5. A comparison of REE in bauxite-kaolin versus REE in granite-regolith

Several similarities and differences were noted between the results in this study and those previously reported for REE occurrences in granite-regolith deposits (Li and Zhou, 2020; Li et al., 2017, 2019, Li et al., 2020, Li and Zhou, 2020; Xu et al., 2017; Sanematsu and Watanabe, 2016; Chi and Jun, 2011; Bao and Zhao, 2008; Wu et al., 1990; Ren, 1985). Similarities between the deposits include REE enrichments relative to UCC and REE fractionation signatures such as Ce/Ce* anomalies. Ce/Ce* anomalies present in granite-regolith are positive anomalies in upper horizons and negative anomalies in lower horizons (Zuoping and Chuanxian, 1996; Sanematsu and Watanabe, 2016; Li et al., 2017; Xu et al., 2017). This trend was also observed in the bauxite-kaolin section studied herein. The strong, positive Ce/Ce* anomaly was observed at the top portion of bauxite zone, with negative Ce/Ce* anomalies in all zones below. There anomalies were attributed to the redox sensitivity for Ce compared to other LREE. Ion-exchangeable REE generally show strong Ce anomalies and reflect whole-rock REE contents dominated by ion-exchangeable REE (Wu et al., 1990; Sanematsu et al., 2015).

Prominent differences between bauxite-kaolin and granite-regolith REE focus on the selectivity HREE and patterns of REE distribution within the bauxite zone. In granite-regolith deposits where kaolinite is a dominant clay mineral, there was preferential uptake for LREE through ion-adsorption reactions (Sholkovitz, 1992). Greater LREE contents are often observed through granite-regolith profiles (Li et al., 2019; Bao and Zhao, 2008). In contrast, the bauxite-kaolin section in this study showed opposite trends. Several factors are responsible for the differences in REE selectivity (Text S9). While granite-regolith deposits dominated by kaolinite favor LREE adsorption, the bauxite-kaolin deposit in this study shows dominantly gibbsite mineral content (i.e. bauxite zone). It is possible that LREE and HREE uptake on gibbsite vs kaolinite was different. For example, HREE are favored as inner-sphere complexes on the gibbsite surface (Borst et al., 2020), which warrants future research.

Overall, the whole rock enrichment in HREE (low La/Yb_N values) and 2–3 times greater ion-exchangeable HREE contents were shown in the bauxite-kaolin profile of this study. Organic ligand complexation was a possible mechanism facilitating REE accumulations in the lowermost portion of the lower kaolin zone. The high concentration of REE in these organic-rich, lignitic clays represents another significant difference when compared to granite-regolith profiles where organic-rich materials are present only at the uppermost horizons (e.g. soil).

5. Conclusions

Bauxites hosted within larger lenses of kaolin occur within late Cretaceous to Eocene sedimentary strata across portions of Georgia and eastern Alabama (USA) in the Southeast Upper Coastal Plain. These deposits were formed through chemical weathering ("bauxitization") of older kaolinite-rich sedimentary strata overlain by younger kaolintic sediments. The bauxite zones from the Andersonville bauxite-kaolin deposit contained highly weathered rocks, typified by intact pisolites and whole rock gibbsite mineral contents exceeding 50%. Several major changes in whole rock mineralogy, major/minor oxide, trace element, and REE geochemistry occurred during the formation of the deposit. These trends were consistent with other occurrences of bauxite-kaolin deposits in the Upper Coastal Plain (Table S8, S9, Fig. S7-S9).

Al_2O_3 and insoluble elements (Zr and Ti) were enriched in the bauxite zones, while alkali and alkaline elements were depleted. HREE concentrations remained relatively unchanged, while LREE were depleted. The fractionation of the REE was further observed by changes in La/Yb_N values and the formation of Ce/Ce* anomalies. During the formation of the bauxite zone, REE were released into the weathering solutions which facilitated sorption with kaolinite minerals at lower zones. The immobility in Ce and Sc contents relative to all other REE

were noteworthy.

Sc contents across the entire section were <3% ion-exchangeable. Sc was hypothesized to be hosted by Fe-oxyhydroxide minerals and unrelated to sorption with kaolinite. The immobility of Ce was firstly shown as strongly positive Ce/Ce* anomalies (1.3) in the top portion of the bauxite zone, and negative Ce/Ce* anomalies (0.8) in the bottom portion. Ce/LREE ratios for ion-exchangeable contents ranged from 0.1 to 0.4 in the bauxite zone. These further indicated Ce immobility attributed to fractionation from the other LREE in the top portion of the bauxite zone. Ce was readily oxidized as highly insoluble CeO_2 and preferentially retained in the top portion of the bauxite zone while the other LREE migrated (in solutions) down to lower zones of where they were accumulated.

The first zone of accumulation represented a transition from gibbsite-rich strata (up to 67 wt% gibbsite) to kaolinite-rich strata at (≤5 wt% gibbsite) at the base of the bauxite zone. At this transition, the remobilized REE were sorbed on kaolinite surfaces, leading to sizable ion-exchangeable REE contents at 15–36% (excluding Ce and Sc): 15–17% for LREE, ~29% for ΣTb-Lu, and ~36% for Y. In the overlying bauxite zone, these ion-exchangeable contents were substantially lower (generally <10%).

While the first accumulation zone at the base of the bauxite showed large gains in ion-exchangeable REE contents, these gains were not sufficient to be observed as enrichment in whole rock ΣREE relative to UCC values. The remaining portions of the remobilized REE led to development of a second zone of accumulation in the lignitic clay at the base of the section within the lower kaolin zone. This second accumulation zone contained elevated ion-exchangeable REE contents ranging at 11–33% (excluding Ce and Sc): 11–12% for LREE, ~28% for ΣTb-Lu, and ~33% for Y. The whole rock ΣREE accumulations were ~460 ppm (~250% relative to UCC) and were thus observed as noteworthy REE enrichment.

The deposit model for the bauxite-kaolin deposit (sedimentary origin) type bears resemblance to the granite-regolith deposit type: a zone of depletion (leaching) underlain by a zone of enrichment (accumulation). The most conspicuous difference between these deposit models would be the sedimentary origin of the bauxite-kaolin deposit.

The character of the REE enrichments in this bauxite-kaolin deposit (sedimentary origin) type at Andersonville drew several other lines for comparison with the granite-regolith deposit type:

1. Ce/Ce* anomalies occur above the zones of REE accumulation in both deposit types.
2. Ion-exchangeable REE were sorbed onto clay minerals in zones of REE accumulation and accounted for sizable fractions of the total REE in both deposit types.
3. The granite-regolith deposit type contains more complex clay mineralogy (e.g. smectite, halloysite) with greater sorption capacity than the chiefly kaolinite/gibbsite clay mineralogy of the bauxite-kaolin deposit type.
4. HREE were evidently favored for accumulation in the bauxite-kaolin deposit type due to gibbsite mineral contents.
5. Organic-rich horizons in the granite-regolith deposit type are limited to the uppermost portions (e.g. soil horizons) and are stratigraphically disconnected from the zones of REE accumulation. However, the sedimentary origin of the studied bauxite-kaolin deposit permits consideration of organic materials stratigraphically linked to zones of REE accumulation. These associations and the results of this study highlight the potential role that organic ligands play during REE precipitation and sorption processes.

The results of this study highlight the movement of dissolved REE and accumulations as sorbed species, warranting further research into REE occurrences in clay deposits of sedimentary origin which have been underexplored compared to granite-regolith REE deposits.

CRediT authorship contribution statement

Anthony Boxleiter: Writing – review & editing, Writing – original draft, Visualization, Methodology, Investigation, Formal analysis, Data curation, Conceptualization. **Yinghao Wen:** Writing – review & editing, Supervision, Methodology, Formal analysis, Data curation. **Yuanzhi Tang:** Writing – review & editing, Supervision, Resources, Project administration, Methodology, Funding acquisition. **W. Crawford Elliott:** Writing – review & editing, Writing – original draft, Supervision, Project administration, Methodology, Investigation, Conceptualization.

Declaration of competing interest

The authors declare the following financial interests/personal relationships which may be considered as potential competing interests: Yuanzhi Tang reports financial support was provided by National Science Foundation. W. Crawford Elliott reports financial support was provided by National Science Foundation. Anthony Boxleiter reports a relationship with Imerys that includes: employment. W. Crawford Elliott has patent #Extracting rare earth elements from a gangue heavy fraction, US Patent No. 10,688,501 issued to Georgia State University Research Foundation, Thiele Kaolin Company. W. Crawford Elliott is on the Editorial Board, Chemical Geology. All other authors declare that they have no known competing financial interests or personal relationships that could have appeared to influence the work reported in this paper.

Data availability

All data used to prepare this paper are given in the text of in the Supplementary Information.

Acknowledgements

Yuanzhi Tang acknowledges support by NSF Grant # 2327660. W. Crawford Elliott acknowledges support by NSF Grant # 2327659. A portion of the laboratory analyses were performed at the Georgia Tech Institute for Electronics and Nanotechnology, a member of the National Nanotechnology Coordinated Infrastructure (NNCI), supported by NSF Grant # ECCS-2025462. Core sample collection and a portion of the laboratory work was supported by Imerys.

Appendix A. Supplementary data

Supplementary data to this article can be found online at https://doi.org/10.1016/j.chemgeo.2024.122151.

References

Aubert, D., Stille, P., Probst, A., 2001. REE fractionation during granite weathering and removal by waters and suspended loads: Sr and Nd isotopic evidence. Geochim. Cosmochim. Acta 65 (3), 387–406. https://doi.org/10.1016/S0016-7037(00)00546-9.

Austin, R., 1972. The Origin of the Kaolin and Bauxite Deposits of Twiggs, Wilkinson, and Washington Counties, Georgia [Ph.D. Dissertation]. University of Georgia.

Baioumy, H., Gilg, H.A., 2011. Pisolitic flint kaolin from Kalabsha, Egypt: A laterite-derived facies. Sediment. Geol. 236 (1), 141–152. https://doi.org/10.1016/j.sedgeo.2011.01.002.

Bao, Z., Zhao, Z., 2008. Geochemistry of mineralization with exchangeable REY in the weathering crusts of granitic rocks in South China. Ore Geol. Rev. 33 (3), 519–535. https://doi.org/10.1016/j.oregeorev.2007.03.005.

Bern, C.R., Shah, A.K., Benzel, W.M., Lowers, H.A., 2016. The distribution and composition of REE-bearing minerals in placers of the Atlantic and Gulf coastal plains, USA. J. Geochem. Explor. 162, 50–61. USGS Publications Warehouse. https://doi.org/10.1016/j.gexplo.2015.12.011.

Borst, A., Smith, M., Finch, A., Estrade, G., Villanova-de-Benavent, C., Nason, P., Marquis, E., Goodenough, K., Xu, C., Kynicky, J., Geraki, K., 2020. Adsorption of rare earth elements in regolith-hosted clay deposits. Nat. Commun. 11 https://doi.org/10.1038/s41467-020-17801-5.

Boxleiter, A., Elliott, W.C., 2023. Rare-Earth Minerals in Kaolin Ore, Mine Tailings, and Sands – Central Georgia, Upper Coastal Plain. Clay Clay Miner. 71 (3), 274–308. https://doi.org/10.1007/s42860-023-00235-7.

Brahim, J.A., Hak, S.A., Achiou, B., Boulif, R., Beniazza, R., Benhida, R., 2022. Kinetics and mechanisms of leaching of rare earth elements from secondary resources. Miner. Eng. 177, 107351 https://doi.org/10.1016/j.mineng.2021.107351.

Bunzli, J.-C., 2013. Lanthanides in Kirk-Othmer Encyclopedia of Chemical Technology. John Wiley & Sons, Ltd. https://onlinelibrary.wiley.com/doi/abs/10.1002/0471238961.1201142019010215.a01.pub3.

Burst, J.F., 1974. Genetic Relationship of the Andersonville, Georgia, and Eufaula, Alabama, Bauxitic Kaolin Areas, 256. Society of Mining Engineers, AIME, pp. 137–143.

Chakhmouradian, A.R., Wall, F., 2012. Rare Earth elements: Minerals, Mines, Magnets (and more). Elements 8 (5), 333–340. https://doi.org/10.2113/gselements.8.5.333.

Chasse, M., Griffin, W.L., O'Reilly, S.Y., Calas, G., 2019. Australian laterites reveal mechanisms governing scandium dynamics in the critical zone. Geochim. Cosmochim. Acta 260, 292–310. https://doi.org/10.1016/j.gca.2019.06.036.

Cheshire, M., 2011. Isotopic and Geochemical Composition of the Georgia Kaolins: Insights into Formation and Diagenetic Conditions. Indiana University.

Cheshire, M.C., Bish, D.L., Brassell, S.C., 2012. Organic Geochemical Composition of the Georgia Kaolins: Insights into Formation and Diagenetic Conditions. Clay Clay Miner. 60 (4), 420–439. https://doi.org/10.1346/CCMN.2012.0600408.

Cheshire, M., Bish, D., Cahill, J., Kertesz, V., Stack, A., 2018. Geochemical Evidence for Rare-Earth Element Mobilization during Kaolin Diagenesis. ACS Earth and Space Chemistry 2. https://doi.org/10.1021/acsearthspacechem.7b00124.

Chi, R., Jun, T., 2011. Weathered crust elution deposited rare earth ores. Weathered Crust Elutiondeposited Rare Earth Ores 1–308.

Cofer, H.E., Manker, J.P., 1983. Geology and Resources of the Andersonville, Georgia, Kaolin and Bauxite District (Report 83–580; Open-File Report). USGS Publications Warehouse. https://doi.org/10.3133/ofr83580.

Condie, K.C., 1991. Another look at rare earth elements in shales. Geochim. Cosmochim. Acta 55 (9), 2527–2531. https://doi.org/10.1016/0016-7037(91)90370-K.

Connelly, N.G., Damhus, T., Hartshorn, R.M., Hutton, A. T. (Eds.)., 2005. Nomenclature of Inorganic Chemistry: IUPAC Recommendations 2005. The Royal Society of Chemistry.

Elliott, W.C., Gardner, D.J., Malla, P., Riley, E.D., 2018. A new look at the occurrences of the rare-earth elements in the Georgia Kaolins. Clay Clay Miner. 66, 245–260. https://doi.org/10.1346/CCMN.2018.064096.

Fedo, C., Nesbitt, H., Young, G., 1995. Unraveling the effects of potassium metasomatism in sedimentary rocks and paleosols, with implications for paleoweathering conditions and provenance. Geology 23, 921–924. https://doi.org/10.1130/0091-7613(1995)023<0921:UTEOPM>2.3.CO;2.

Feng, M., Ngwenya, B.T., Wang, L., Li, W., Olive, V., Ellam, R.M., 2011. Bacterial dissolution of fluorapatite as a possible source of elevated dissolved phosphate in the environment. Geochim. Cosmochim. Acta 75 (19), 5785–5796. https://doi.org/10.1016/j.gca.2011.07.019.

Fortier, S.M., Nassar, N.T., Lederer, G.W., Brainard, J., Gambogi, J., McCullough, E.A., 2018. Draft critical mineral list—Summary of methodology and background information—U.S. Geological Survey technical input document in response to Secretarial Order no. 3359 (Report 2018–1021; Open-File Report, p. 26). USGS Publications Warehouse. https://doi.org/10.3133/ofr20181021.

Gamaletsos, P., Godelitsas, A., Filippidis, A., Pontikes, Y., 2018. The rare Earth elements potential of Greek Bauxite active Mines in the Light of a Sustainable REE demand. Journal of Sustainable Metallurgy 5, 20–47. https://doi.org/10.1007/s40831-018-0192-2.

Gromet, L.P., Haskin, L.A., Korotev, R.L., Dymek, R.F., 1984. The "north American shale composite": its compilation, major and trace element characteristics. Geochim. Cosmochim. Acta 48 (12), 2469–2482. https://doi.org/10.1016/0016-7037(84)90298-9.

Hack, J.T., 1982. Physiographic divisions and differential uplift in the Piedmont and Blue Ridge. US Geological Survey 1265, 49. https://doi.org/10.3133/pp1265.

He, Z., Zhang, Z., Yu, J., Zhou, F., Xu, Y., Xu, Z., Chen, Z., Chi, R., 2016. Kinetics of column leaching of rare earth and aluminum from weathered crust elution-deposited rare earth ore with ammonium salt solutions. Hydrometallurgy 163, 33–39. https://doi.org/10.1016/j.hydromet.2016.02.016.

Hinckley, D.N., 1965. Mineralogical and chemical variations in the kaolin deposits of the coastal plain of Georgia and South Carolina. Am. Mineral. 50 (11–12), 1865–1883.

Huddlestun, P.P., 1982. The development of the stratigraphic terminology of the Claibornian and Jacksonian marine deposits of western South Carolina and eastern Georgia. In: Nystrom Jr., P.G., Willoughby, R.H. (Eds.), Geological Investigations Related to the Stratigraphy in the Kaolin Mining District, Aiken County, South Carolina (Carolina Geological Society Field Trip Guidebook for 1982). South Carolina Geological Survey, Columbia, S.C., pp. 21–33

Huddlestun, P.F., Hetrick, J.H., 1991. The stratigraphic framework of the Fort Valley plateau and the central Georgia kaolin district. Georgia Geological Society Guidebook, 26th Annual Field Trip 11 (1), 119. October, 1991.

Kadir, S., Külah, T., Erkoyun, H., Uyanık, N.Ö., Eren, M., Elliott, W.C., 2021. Mineralogy, geochemistry, and genesis of bentonites in Upper cretaceous pyroclastics of the Bereketli member of the Reşadiye Formation, Reşadiye (Tokat), Turkey. Appl. Clay Sci. 204, 106024 https://doi.org/10.1016/j.clay.2021.106024.

Kloprogge, T., Ruan, H., Frost, R., 2002. Thermal decomposition of bauxite minerals: infrared emission spectroscopy of gibbsite, boehmite and diaspore. J. Mater. Sci. 37 https://doi.org/10.1023/A:1014303119055.

Lang, W.B., Warren, W.C., Thompson, R.M., Overstreet, E.F., 1965. Bauxite and Kaolin Deposits of the Irwinton District, Georgia (Report 1199J; Bulletin). USGS Publications Warehouse. https://doi.org/10.3133/b1199J.

Li, M.Y.H., Zhou, M.-F., 2020. The role of clay minerals in forming the regolith-hosted heavy rare earth element deposits. Am. Mineral. 105, 92–108. https://doi.org/10.2138/am-2020-7061.

Li, Y.H.M., Zhao, W.W., Zhou, M.-F., 2017. Nature of parent rocks, mineralization styles and ore genesis of regolith-hosted REE deposits in South China: an integrated genetic model. J. Asian Earth Sci. 148, 65–95. https://doi.org/10.1016/j.jseaes.2017.08.004.

Li, M.Y.H., Zhou, M.-F., Williams-Jones, A.E., 2019. The Genesis of Regolith-Hosted Heavy rare Earth Element deposits: Insights from the World-Class Zudong Deposit in Jiangxi Province, South China. Econ. Geol. 114 (3), 541–568. https://doi.org/10.5382/econgeo.4642.

Li, M.Y.H., Zhou, M.-F., Williams-Jones, A.E., 2020. Controls on the Dynamics of rare Earth elements during Subtropical Hillslope Processes and Formation of Regolith-Hosted Deposits. Econ. Geol. 115 (5), 1097–1118. https://doi.org/10.5382/econgeo.4727.

Long, K., Gosen, B.S., Foley, N., Cordier, D., 2010. The principal rare earth elements deposits of the United States. USGS Scientific Investigations Report 2010-5220, 96. http://pubs.usgs.gov/sir/2010/5220/.

Long, P., Wang, G., Zhang, C., Yang, Y., Cao, X., Shi, Z., 2020. Kinetics model for leaching of ion-adsorption type rare earth ores. J. Rare Earths 38 (12), 1354–1360. https://doi.org/10.1016/j.jre.2019.11.011.

Lukas, T.C., Loughnan, F.C., Eades, J.L., 1983. Origin of bauxite at Eufaula, Alabama, USA. In: Clay Minerals, 18(2), 127–138. Core, Cambridge. https://doi.org/10.1180/claymin.1983.018.2.02.

Ma, L., Jin, L., Brantley, S.L., 2011. How mineralogy and slope aspect affect REE release and fractionation during shale weathering in the Susquehanna/Shale Hills critical Zone Observatory. Chem. Geol. 290 (1), 31–49. https://doi.org/10.1016/j.chemgeo.2011.08.013.

Mamedov, V., Boeva, N., Makarova, M., E.S., S., & Melnikov, P., 2022. The Problem of the Formation of Boehmite and Gibbsite in Bauxite-Bearing Lateritic Profiles. Minerals 12, 389. https://doi.org/10.3390/min12030389.

McLennan, S.M., Taylor, S.R., 2012. Geology, Geochemistry and Natural Abundances. In: Encyclopedia of Inorganic and Bioinorganic Chemistry. American Cancer Society. https://doi.org/10.1002/9781119951438.eibc2004.

Middelburg, J., Weijden, C., Woittiez, J., 1988. Chemical processes affecting the mobility of major, minor and trace elements during weathering of granitic rocks. Chem. Geol. 68, 253–273. https://doi.org/10.1016/0009-2541(88)90025-3.

Migaszewski, Z., Gałuszka, A., 2015. The Characteristics, Occurrence, and Geochemical Behavior of rare Earth elements in the Environment: A Review. Crit. Rev. Environ. Sci. Technol. 45, 429–471. https://doi.org/10.1080/10643389.2013.866622.

Minato, H., 1988. Dehydration energy of halloysite by means of D. S. C. Methods with the relationships of its mineralogy and modes of occurrence. Thermochim. Acta 135, 279–283. https://doi.org/10.1016/0040-6031(88)87398-2.

Mioduski, T., 1993. Covalency of Sc(III), Y(III), Ln(III) and an(III) as manifested in the enthalpies of solution of anhydrous rare earth halides. J. Radioanal. Nucl. Chem. 176 (5), 371–382. https://doi.org/10.1007/bf02163384.

Moldoveanu, G.A., Papangelakis, V.G., 2012. Recovery of rare earth elements adsorbed on clay minerals: I. Desorption mechanism. Hydrometallurgy 117–118, 71–78. https://doi.org/10.1016/j.hydromet.2012.02.007.

Moldoveanu, G.A., Papangelakis, V.G., 2013. Recovery of rare earth elements adsorbed on clay minerals: II. Leaching with ammonium sulfate. Hydrometallurgy 131–132, 158–166. https://doi.org/10.1016/j.hydromet.2012.10.011.

Moldoveanu, G., Papangelakis, V., 2016. An overview of rare-earth recovery by ion-exchange leaching from ion-adsorption clays of various origins. Mineral. Mag. 80, 63–76. https://doi.org/10.1180/minmag.2016.080.051.

Mongelli, G., Boni, M., Oggiano, G., Mameli, P., Sinisi, R., Buccione, R., Mondillo, N., 2017. Critical metals distribution in Tethyan karst bauxite: the cretaceous Italian ores. Ore Geol. Rev. 86, 526–536. https://doi.org/10.1016/j.oregeorev.2017.03.017.

Murakami, H., Ishihara, S., 2008. REE Mineralization of Weathered Crust and Clay Sediment on Granitic Rocks in the Sanyo Belt, SW Japan and the Southern Jiangxi Province, China. Resour. Geol. 58 (4), 373–401. https://doi.org/10.1111/j.1751-3928.2008.00071.x.

Murray, H., 2007. Applied clay mineralogy: Occurrences, processing, and application of kaolins, bentonites, palygorskite-sepiolite, and common clays. Elsevier, p. 180.

Nesbitt, H.W., Young, G., 1982. Early Proterozoic climates and plate motions inferred from major element chemistry of lutites. Nature 299. https://doi.org/10.1038/299715a0.

Norton, S.A., 1973. Laterite and Bauxite Formation. Econ. Geol. 68 (3), 353–361. https://doi.org/10.2113/gsecongeo.68.3.353.

Nystrom Jr., P.G., Willoughby, R.H., Price, L.K., 1991. Cretaceous and Tertiary stratigraphy of the upper coastal plain, South Carolina. In: Horton Jr., J.W., Zullo, V. A. (Eds.), The geology of the Carolinas: Carolina Geological Society, 50th Anniversary Volume, pp. 221–240.

Owens, J.P., Gohn, G.S., 1985. Depositional history of the cretaceous series in the U.S. Atlantic coastal plain: Stratigraphy, paleoenvironments, and tectonic controls of sedimentation. In: Poag, C.W. (Ed.), Geologic Evolution of the United States Atlantic Margin. Van Nostrand Reinhold Co., pp. 25–85

Patterson, S.H., Murray, H.H., 1984. Kaolin, Refractory Clay, Ball Clay, and Halloysite in North America, Hawaii, and the Caribbean Region (Report 1306; Professional Paper, p. 56). USGS Publications Warehouse. https://doi.org/10.3133/pp1306.

Pavich, M.J., 1989. Regolith residence time and the concept of surface age of the Piedmont "Peneplain". Geomorphology 2, 181–196 https://doi.org/10.1016/0169-555X(89)90011–1.

Piper, D.Z., 1974. Rare earth elements in the sedimentary cycle: A summary. Chem. Geol. 14 (4), 285–304. https://doi.org/10.1016/0009-2541(74)90066-7.

Ren, X., 1985. A brief account of rare earth mineralization in China. In: Xu, Q. (Ed.), New Frontiers in REE Science and Applications: Beijing. Science Press, China, pp. 39–41.
Rodgers, J.L., Nicewander, W.A., 1988. Thirteen Ways to look at the Correlation Coefficient. The American Statistician, 42(1). JSTOR, pp. 59–66. https://doi.org/10.2307/2685263.
Ruan, C., Jun, T., Zhongjun, L., Cui, P., Yuanxin, W., Shirong, L., Cunwen, W., Zhou, Z.A., 2005. Existing State and Partitioning of rare Earth on Weathered Ores. J. Rare Earths 23, 756–759.
Rudnick, R., Gao, S., 2003. Composition of the Continental Crust. Treatise on Geochem. 3, 1–64. https://doi.org/10.1016/B0-08-043751-6/03016-4.
Sanematsu, K., Watanabe, Y., 2016. Characteristics and Genesis of Ion Adsorption-Type rare Earth Element Deposits. In: Verplanck, P.L., Hitzman, M.W. (Eds.), Rare Earth and Critical Elements in Ore Deposits, vol. 18. Society of Economic Geologists, pp. 55–79. https://doi.org/10.5382/Rev.18.03.
Sanematsu, K., Kon, Y., Imai, A., 2015. Influence of phosphate on mobility and adsorption of REEs during weathering of granites in Thailand. J. Asian Earth Sci. 111, 14–30. https://doi.org/10.1016/j.jseaes.2015.05.018.
Shannon, R., 1976. Revised Effective Ionic Radii and Systematic Study of Inter Atomic Distances in Halides and Chalcogenides. Acta Crystallogr. A 32, 751–767. https://doi.org/10.1107/s0567739476001551.
Sholkovitz, E.R., 1992. Chemical evolution of rare earth elements: Fractionation between colloidal and solution phases of filtered river water. Earth Planet. Sci. Lett. 114 (1), 77–84. https://doi.org/10.1016/0012-821X(92)90152-L.
Smith, R.W., 1929. Sedimentary Kaolins of the Coastal Plain of Georgia: Georgia Geol. Survey Bulletin 44, 35–37.
Stull, R.T., Bole, G.A., 1926. Beneficiation and utilization of Georgia Clays: Bureau of Mines. Bulletin 252, 6.
Tang, J., Johannesson, K.H., 2003. Speciation of rare earth elements in natural terrestrial waters: Assessing the role of dissolved organic matter from the modeling approach. Geochim. Cosmochim. Acta 67 (13), 2321–2339. https://doi.org/10.1016/S0016-7037(02)01413-8.
Tang, J., Johannesson, K.H., 2010. Rare earth elements adsorption onto Carrizo sand: Influence of strong solution complexation. Chem. Geol. 279 (3), 120–133. https://doi.org/10.1016/j.chemgeo.2010.10.011.
Taunton, A., Welch, S., Banfield, J., 2000. Geomicrobiological controls on light rare earth element, Y and Ba distributions during granite weathering and soil formation. J. Alloys Compd. 303–304, 30–36. https://doi.org/10.1016/S0925-8388(00)00597-1.
Teitler, Y., Cathelineau, M., Ulrich, M., Ambrosi, J.P., Munoz, M., Sevin, B., 2019. Petrology and geochemistry of scandium in New Caledonian Ni-Co laterites. J. Geochem. Explor. 196, 131–155. https://doi.org/10.1016/j.gexplo.2018.10.009.
Tepe, N., Bau, M., 2016. Behavior of rare earth elements and yttrium during simulation of arctic estuarine mixing between glacial-fed river waters and seawater and the impact of inorganic (nano-)particles. Chem. Geol. 438, 134–145. https://doi.org/10.1016/j.chemgeo.2016.06.001.
Tessier, A., Campbell, P.G.C., Bisson, M., 1979. Sequential extraction procedure for the speciation of particulate trace metals. Anal. Chem. 51 (7), 844–851. https://doi.org/10.1021/ac50043a017.
Van Gosen, B.S., Verplanck, P.L., Emsbo, P., 2019. Rare earth element mineral deposits in the United States. 24. USGS Publications Warehouse. https://doi.org/10.3133/cir1454.
Verplanck, P.L., Van Gosen, B.S., Seal II, R.R., McCafferty, A.E., 2014. A Deposit Model for Carbonatite and Peralkaline Intrusion-Related Rare Earth Element Deposits: Chapter J in Mineral Deposit Models for Resource Assessment (Report 2010-5070J; Scientific Investigations Report, p. 72). USGS Publications Warehouse. https://doi.org/10.3133/sir20105070J.
Vind, J., Malfliet, A., Bonomi, C., Paiste, P., Sajó, I.E., Blanpain, B., Tkaczyk, A.H., Vassiliadou, V., Panias, D., 2018. Modes of occurrences of scandium in Greek bauxite and bauxite residue. Miner. Eng. 123, 35–48. https://doi.org/10.1016/j.mineng.2018.04.025.
Voicu, G., Bardoux, M., 2002. Geochemical behavior under tropical weathering of the Barama–Mazaruni greenstone belt at Omai gold mine, Guiana Shield. Appl. Geochem. 17 (3), 321–336. https://doi.org/10.1016/S0883-2927(01)00085-3.
Voicu, G., Bardoux, M., 2002. Geochemical behavior under tropical weathering of the Barama–Mazaruni greenstone belt at Omai gold mine, Guiana Shield. Applied Geochemistry 17 (3), 321–336. https://doi.org/10.1016/S0883-2927(01)00085-3.
Wall, F., 2021. Rare Earth elements. In: Alderton, D., Elias, S.A. (Eds.), Encyclopedia of Geology (Second Edition), Second edition. Academic Press, pp. 680–693. https://doi.org/10.1016/B978-0-08-102908-4.00101-6.
Wan, Y., Liu, C., 2006. The effect of humic acid on the adsorption of REEs on kaolin. Colloids Surf. A Physicochem. Eng. Asp. 290 (1), 112–117. https://doi.org/10.1016/j.colsurfa.2006.05.010.
Wang, Z., Li, M.Y.H., Liu, Z., Zhou, M.-F., 2021. Scandium: Ore deposits, the pivotal role of magmatic enrichment and future exploration. Ore Geol. Rev. 128, 103906 https://doi.org/10.1016/j.oregeorev.2020.103906.
Warren, W.C., Clark, L.D., 1965. Bauxite Deposits of the Eufaula District, Alabama (Report 1199E; Bulletin). USGS Publications Warehouse. https://doi.org/10.3133/b1199E.
Wen, Y., Hu, L., Boxleiter, A., Li, D., Tang, Y., 2023. Rare Earth elements Recovery and Waste Management of Municipal Solid Waste Incineration Ash. ACS Sustainable Resource Management. https://doi.org/10.1021/acssusresmgt.3c00026.
Williams-Jones, A.E., Vasyukova, O.V., 2018. The Economic Geology of Scandium, the Runt of the rare Earth Element Litter. Econ. Geol. 113 (4), 973–988. https://doi.org/10.5382/econgeo.2018.4579.
Wilson, M.J., 2013. Rock-Forming Minerals, , 2nd editionVol. 3c. Sheet Silicates-Clay Minerals.
Wood, S.A., 1990. The aqueous geochemistry of the rare-earth elements and yttrium: 1. Review of available low-temperature data for inorganic complexes and the inorganic REE speciation of natural waters. Chem. Geol. 82, 159–186. https://doi.org/10.1016/0009-2541(90)90080-Q.
Wu, C., Huang, D., Guo, Z., 1990. REE Geochemistry in the Weathered Crust of Granites, Longnan Area, Jiangxi Province. Acta Geologica Sinica - English Edition 3 (2), 193–209. https://doi.org/10.1111/j.1755-6724.1990.mp3002006.x.
Wu, C., Yuan, Z., Bai, G., 1996. Rare earth deposites in China. W: rare Earth Minerals: Chemistry, origin and ore deposits. Rare Earth Minerals: Chemistry, Origin and Ore Deposits 7, 281–306.
Xiao, Y., Chen, Y., Feng, Z., Huang, X., Huang, L., Long, Z., Cui, D., 2015. Leaching characteristics of ion-adsorption type rare earths ore with magnesium sulfate. Trans. Nonferrous Metals Soc. China 25 (11), 3784–3790. https://doi.org/10.1016/S1003-6326(15)64022-5.
Xu, C., Kynicky, J., Smith, M., Kopřiva, A., Brtnický, M., Urubek, T., Yang, Y., Zhao, Z., He, C., Wenlei, S., 2017. Origin of heavy rare earth mineralization in South China. Nat. Commun. 8 https://doi.org/10.1038/ncomms14598.
Yan, P., Zhang, G., Yang, Y., Mclean, A., 2019. Characterization and Pre-concentration of Scandium in Low-Grade Magnetite Ore. JOM 71. https://doi.org/10.1007/s11837-019-03541-5.
Yang, X.J., Lin, A., Li, X.-L., Wu, Y., Zhou, W., Chen, Z., 2013. China's ion-adsorption rare earth resources, mining consequences and preservation. Environmental Development 8, 131–136. https://doi.org/10.1016/j.envdev.2013.03.006.
Yang, S., Wang, Q., Liu, X., Kan, Z., Santosh, M., Deng, J., 2022. Global spatio-temporal variations and metallogenic diversity of karst bauxites and their tectonic, paleogeographic and paleoclimatic relationship with the Tethyan realm evolution. Earth Sci. Rev. 233, 104184 https://doi.org/10.1016/j.earscirev.2022.104184.
Yusoff, Z.M., Ngwenya, B.T., Parsons, I., 2013. Mobility and fractionation of REEs during deep weathering of geochemically contrasting granites in a tropical setting, Malaysia. Chem. Geol. 349–350, 71–86. https://doi.org/10.1016/j.chemgeo.2013.04.016.
Zapp, A.D., 1965. Bauxite Deposits of the Andersonville District, Georgia (Report 1199G; Bulletin). USGS Publications Warehouse. https://doi.org/10.3133/b1199G.
Zhu, B., Fang, B., Li, X., 2010. Dehydration reactions and kinetic parameters of gibbsite. Ceram. Int. 36 (8), 2493–2498. https://doi.org/10.1016/j.ceramint.2010.07.007.
Zielinski, R.A., 1982. The mobility of uranium and other elements during alteration of rhyolite ash to montmorillonite: A case study in the Troublesome Formation, Colorado, U.S.A. Chem. Geol. 35 (3), 185–204. https://doi.org/10.1016/0009-2541(82)90001-8.
Zuoping, Z., Chuanxian, L., 1996. The behaviour of rare-earth elements (REE) during weathering of granites in southern Guangxi, China. Chin. J. Geochem. 15 (4), 344–352. https://doi.org/10.1007/BF02867008.